NASA TECHNICAL NOTE

NASA TN D-3278

CALIBRATION EXPERIENCE IN THE LANGLEY HOTSHOT TUNNEL FOR MACH NUMBERS FROM 12 TO 26

by Charles G. Miller III, Theodore R. Creel, Jr., and Fred M. Smith

Langley Research Center
Langley Station, Hampton, Va.

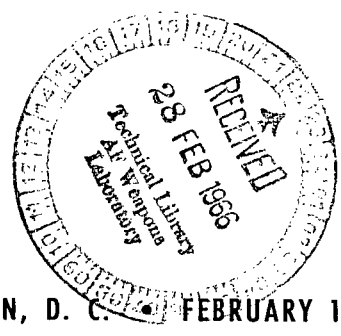

NATIONAL AERONAUTICS AND SPACE ADMINISTRATION • WASHINGTON, D. C. • FEBRUARY 1966

NASA TN D-3278

CALIBRATION EXPERIENCE IN THE LANGLEY HOTSHOT TUNNEL FOR MACH NUMBERS FROM 12 TO 26

By Charles G. Miller III, Theodore R. Creel, Jr., and Fred M. Smith

Langley Research Center
Langley Station, Hampton, Va.

NATIONAL AERONAUTICS AND SPACE ADMINISTRATION

For sale by the Clearinghouse for Federal Scientific and Technical Information
Springfield, Virginia 22151 – Price $2.00

CALIBRATION EXPERIENCE IN THE LANGLEY HOTSHOT TUNNEL FOR MACH NUMBERS FROM 12 TO 26

By Charles G. Miller III, Theodore R. Creel, Jr., and Fred M. Smith
Langley Research Center

SUMMARY

Development and calibration results with the Langley hotshot tunnel utilizing an end-firing coaxial-electrode arc-chamber configuration are presented herein. For a 0.100-inch (2.54-millimeter) nozzle throat diameter and arc-chamber stagnation temperatures of approximately 1700° and 2200° K, an axial Mach number gradient of 0.056 per inch (2.2 per meter) was observed for the nozzle length examined (nozzle axial stations ranging from 116.5 inches (2.96 meters) to 150 inches (3.81 meters)). Variation in nozzle throat diameter from 0.025 to 0.500 inch (0.635 to 12.7 millimeters) for stagnation temperatures of 2200° to 2600° K resulted in test-section free-stream Mach numbers of 12 to 26. Boundary-layer-displacement thickness data were observed to be in close agreement with semiempirical predictions for the range of nozzle throat diameters tested; boundary-layer thickness data for nozzle throats corresponding to free-stream Mach numbers of 11.6, 12.6, and 14.5 were in good agreement with predictions of a semiempirical relationship whereas a discrepancy was observed for all other nozzle throats tested. Force and moment coefficients obtained on a blunted cone having a 9° semiapex angle at a Mach number of 20 were in good agreement with results from other hypervelocity facilities. By utilizing a sharp-leading-edge flat plate, a preliminary investigation of nitrogen condensation at a Mach number of approximately 21 showed the condensation onset to occur at a free-stream temperature of 19° K for a free-stream static pressure of approximately 0.001 psi (6.895 newtons per square meter); this compares well with condensation results of other facilities. Flow contamination level was reduced with the new coaxial-electrode arc chamber when compared with the original opposed-electrode arc chamber.

INTRODUCTION

A description of the Langley hotshot tunnel along with a discussion of the early developmental experience and a limited calibration were presented in reference 1. These results were obtained with an arc chamber utilizing opposed electrodes which fired transversely to the tunnel axis. Reference 1 also included a brief description of a new end-firing arc chamber incorporating coaxial electrodes alined with the tunnel axis.

Since the presentation of reference 1, the calibration of the conical nozzle has been extended to include nozzle axial stations ranging from 116.5 to 150 inches (2.96 to 3.81 meters) as compared with 124.4 to 131.8 inches (3.16 to 3.35 meters) in the original calibration. The effect of nozzle throat diameter, which was varied from 0.025 to 0.500 inch (0.635 to 12.7 millimeters), on nozzle-test-section flow parameters was examined at a constant axial station for arc-chamber stagnation temperatures of 2200° to 2600° K. Force and moment coefficients have been obtained for a blunted cone with a 9° semiapex angle and compared with results from several other hypervelocity facilities. A preliminary investigation of nitrogen condensation has been performed with a sharp-leading-edge flat plate. Additional flow contamination results have been obtained for the coaxial-electrode arc chamber and compared with the results obtained for the original electrode configuration (ref. 1).

This presentation includes results from the preceding investigations along with a brief description of pertinent design and development features of the Langley hotshot tunnel with the end-firing, coaxial-electrode arc chamber.

SYMBOLS

$\left(\frac{A}{A^*}\right)_{effective}$	ratio of effective nozzle-to-throat cross-sectional area (mass flow considerations)
$\left(\frac{A}{A^*}\right)_{geometric}$	ratio of geometric nozzle-to-throat cross-sectional area
C_A	axial-force coefficient, F_A/q_1S
C_m	pitching-moment coefficient, M_Y/q_1SD
C_N	normal-force coefficient, F_N/q_1S
d	diameter
D	model base diameter
F_A	axial force
F_N	normal force
h	density altitude
H	enthalpy
L/D	lift-drag ratio
m	mass flow

$\dot{m}$	mass flow rate
M	Mach number
M_Y	pitching moment
N_{Re}	Reynolds number
p	pressure
q	dynamic pressure
r	radius
R	universal gas constant
S	model base area
t	elapsed tunnel run time
T	temperature
v	velocity
x	nozzle axial distance from throat
X	distance along flat-plate surface from leading edge
α	angle of attack
δ	boundary-layer thickness
δ^*	boundary-layer displacement thickness
ϕ	effective nozzle half-angle
μ	coefficient of viscosity
ψ	model bluntness ratio, r_n/r_b
ρ	density, amagats (a relative scale referred to density at 273.16° K and 1 atmosphere of pressure)
σ	ratio of free-stream parameters calculated for velocity-corrected flow to those calculated from uncorrected flow

Subscripts:

1	calculated free-stream conditions
b	model base

calc	calculated using program of reference 6
D	model base diameter
i	arc-chamber conditions preceding arc discharge
n	model nose
r	based on Eckert reference enthalpy
s	flow conditions on flat plate surface
t,1	arc-chamber conditions following arc discharge
t,2	stagnation conditions behind normal shock
vel	calculated using measured free-stream velocity
w	wall conditions
x	nozzle axial distance from throat

Superscripts:

'	extrapolated value at $X^{-1/2} = 0$
*	conditions at nozzle throat

A bar over a symbol denotes average value across inviscid core.

The units used for the physical quantities in this paper are given both in the U.S. Customary Units and the International System of Units (with the exception of temperature and density, which are given only in ^{o}K and amagats (a relative scale referred to density at 273.16^{o} K and 1 atmosphere of pressure), respectively). Conversion factors relating the two systems are given in reference 2, and those used in the present investigation are presented in the following table:

Physical quantity (symbol)	U.S. Customary Unit	Conversion factor (*)	International System of Units
d, D, x, X, r, δ, δ* . .	in.	0.0254	meters (m)
h	ft	0.3048	meters (m)
A, S	in^2	6.452×10^{-4}	sq meters (m^2)
F_A, F_N	lbf	4.448	newtons (N)
m	lbm	0.454	kilograms (kg)
H	ft^2/sec^2	9.290×10^{-2}	sq meter/$second^2$ (m^2/s^2)
$\dot{m}$	lbm/sec	0.454	kilograms/second (kg/s)
M_Y	in-lbf	0.113	meter-newton (m-N)
p, q	lbf/in^2	6.895×10^3	newtons/sq meter (N/m^2)
R	ft^2/sec^2-°K	0.928	sq meters/$second^2$-degrees Kelvin $(m^2/s^2$-°K)
N_{Re}	1/ft	3.283	per meter (1/m)
v	ft/sec	0.3048	meters/second (m/s)
μ	lbm/ft-sec	1.488	newton-second/sq meter $(N\text{-}s/m^2)$

*Multiply value in U.S. Customary Unit by conversion factor to obtain equivalent value in International System of Units.

Temperature and density are presented in degrees Kelvin and amagat units, respectively, throughout this paper.

DESCRIPTION AND OPERATION OF THE LANGLEY HOTSHOT TUNNEL

Tunnel Description

The Langley hotshot tunnel (fig. 1) is a hypervelocity, arc-heated, blow-down facility. The major components of this facility include a capacitor bank with an electrical charging unit, an arc chamber incorporating coaxial electrodes, a 10° total-divergence-angle conical nozzle and test section followed

by a 24-inch-diameter (0.61-m) cylindrical section, a 10° cone-cylinder diffuser, and a 300-cubic-foot (8.49-m^3) vacuum reservoir with vacuum pumps.

The coaxial-electrode arc chamber, which is shown in figure 2, was constructed from a 5-inch (12.7-cm) naval gun barrel having an outside diameter of 13 inches (33 cm) and a wall thickness of approximately 3.5 inches (8.9 cm). The internal volume was about 180 cubic inches ($2.95\ \text{dm}^3$) for the present investigation, but may be changed by using different liner wall thicknesses. The orifice to the nozzle was sealed by a poly[ethylene terephthalate] diaphragm.

Ports were provided for the dump valve, the arc-chamber pressure transducers, and the arc-chamber evacuation system. The initial seals provided for these ports were of the mismatched taper type which required the alinement of fittings to be almost perfect to get an effective seal. Since the arc chamber must be quite frequently disassembled and reassembled, the alinement was difficult to maintain and the seal was less than satisfactory. The seal which was substituted and which has proved to be very satisfactory is shown in figure 2. Note the spherical ends of the steel fittings which press against the soft copper inserts; the spherical-ended fittings compensate for small amounts of misalinement. The seals at the ends of the arc chamber (fig. 2) have proved to be excellent for the pressure and temperature levels presently being encountered (up to 1250 atmospheres ($127\ \text{MN/m}^2$) and 5000° K). The downstream end was sealed with a Fluorogreen ring compressed between the copper liner and the nozzle block. The seal at the upstream end of the arc chamber was improved by adding an adjusting nut (fig. 2) behind the electrode, which pushed the electrodes forward and thereby compressed the insulator between the two main electrodes.

The arc-chamber electrode configuration consisted of two main electrodes and one trigger electrode in a coaxial arrangement. The negative electrode was located on the outside of the assembly. It consisted of a beryllium copper body with that portion of the electrode which was exposed to the gas being made of steel. The positive electrode consisted of a beryllium copper body with that portion of the electrode which was exposed to the hot gas being made of oxygen-free copper.

The electrical energy was conducted from the 1.9×10^3 Btu (2 megajoules) capacitor bank located in the basement beneath the tunnel to the collector (fig. 1) by 72 coaxial cables, each connected to a bank of 10 capacitors. The cables were connected to the collector as shown in reference 1.

In order to alleviate excessive arc-chamber damage, a dump valve was utilized to release residual gases at a predetermined time. The dump valve consisted of a cylindrical body, a piston, a trigger, an adapter, and one pressurizing and four exhaust ports (fig. 2). The dump valve was mounted to the downstream end of the arc chamber.

Removable nozzle throat inserts having throat diameters from 0.025 to 0.500 inch (0.635 to 12.7 mm) were employed to obtain variations in test-section Mach number. Throat erosion over a period of usage was minimized by

constructing the throat inserts of tungsten. The usable life of these inserts was greatly extended by pressing a steel sleeve over the entire length to avoid failure in tension.

All nozzle throat inserts except one had a converging total entrance angle of 22.5° and expanded from the throat into a conical nozzle with a 10° total-divergence angle. The exception was an insert with a throat diameter of 0.100 inch (2.54 mm) for which the total entrance angle was increased to 38°. No significant deviation in test-section results from those obtained with an entrance angle of 22.5° was observed.

The nozzle test section is equipped with opposed 11-inch-diameter (2.79-dm) plate-glass windows; the centers of these windows are at a nozzle axial station of 127 inches (3.23 m). These windows are incorporated into a single-pass schlieren system and also supply means of access to the test model. Because the plate-glass schlieren windows do not conform to the nozzle contour, it was believed that such a discontinuity in nozzle wall geometry might produce disturbances in the nozzle boundary layer, which in turn would affect the inviscid core flow properties. Contoured window blanks conforming to the nozzle contour were tested, but no data discrepancies were observed.

In order to lengthen the tunnel running time and to eliminate any flow fluctuations due to disturbances propagating upstream in the boundary layer, a brief diffuser study was made. Conical diffusers having converging total entrance angles of 8°, 12°, and 16° and ratios of diffuser exit area to cylindrical entrance area of 0.4, 0.5, and 0.55 were employed. A conical diffuser with a 16° total angle and an area ratio of 0.6 and one with a 10° total angle and an area ratio of 0.55 were fabricated with 4-foot (1.22-m) cylindrical after sections. This latter diffuser configuration was found to produce the maximum run time and extended the run time from approximately 40 milliseconds (ref. 1) to approximately 120 milliseconds for a nozzle-throat diameter of 0.100 inch (2.54 mm); it is presently incorporated into the facility.

The 300-cubic-foot (8.49-m^3) vacuum reservoir is evacuated to about 0.00005 psi $(0.345\ \text{N/m}^2)$ in approximately 30 minutes by a rotary piston forepump and a 6-inch (15.25-cm) oil diffusion pump. To compensate for outgassing and possible leaks in the system, a 12-inch (30.5-cm) remotely operated pneumatic valve permits the vacuum pumps to continue pumping on the system until immediately before the tunnel firing.

Operating Procedure

Following evacuation of the nozzle and vacuum chamber to approximately 0.00005 psi $(0.345\ \text{N/m}^2)$, the arc chamber is initially pressurized at ambient temperature with the test gas (nitrogen). A quantity of stored electrical energy is then discharged across the coaxial electrodes when the arc gap is broken down by exploding a trigger wire between the electrodes. The resulting increase in pressure and temperature within the arc chamber results in the rupture of the diaphragm between the arc chamber and evacuated nozzle. The

gas then expands through the diverging conical nozzle into the vacuum chamber. Tunnel running time is terminated approximately 40 to 120 milliseconds after arc discharge depending on the nozzle throat diameter employed.

INSTRUMENTATION

Initial charge pressure in the arc chamber was measured with a Bourdon type gage having an operating range from 0 to 5000 psi (0 to 34.5 MN/m^2). The arc-chamber pressure following arc discharge was monitored by two high-response strain-gage transducers having a full-scale rating of 20 000 psi (138 MN/m^2).

The short running time of the tunnel (40 to 120 milliseconds) and range of test-section pitot and static pressures to be measured (approximately 0.001 to 10.0 psi (6.895 to 6.895 $\times 10^4$ N/m^2)) required pressure instrumentation with very short response times, high sensitivity, and minimum length of orifice tubing. In the present investigation, all test-section pressure measurements were made with double-coil, single-diaphragm, variable-reluctance transducers. (See refs. 3 and 4 for description and theory of operation.) All pressure transducers were excited by 5-volt 20-kilocycle carrier amplifiers. The output signals from the amplifiers drove galvanometers in a light-beam-type oscillograph having a variety of chart speeds.

Present test-section pitot-pressure surveys were made with the 19-probe survey rake shown in figure 3. The findings of reference 5 indicate that the probe geometry of the survey rake (probe ratio of inside diameter to outside diameter of 0.5) used in the present investigation was essentially free from Reynolds number effects for the present regime of flow conditions.

The method of reference 1 for protecting pressure instrumentation from flow contamination was replaced by the contamination trap configuration illustrated in figure 3. Contamination particles entering the pitot tubes impinge on the blank end of the tubes while, according to Pascal's law, the tube pressure is transmitted undiminished throughout the tubing volume. The rake transducers were referenced to a manifold contained within the rake. This manifold was maintained at a constant pressure of approximately 0.0005 psi (3.45 N/m^2) during tunnel firing.

As part of the present investigation, force and moment characteristics were obtained for the blunted cone with a 9° semiapex angle, shown in figure 4(a). A three-component internally mounted, high-frequency response strain-gage balance was employed and is illustrated in figure 4(b). The electrical output signals of the balance were amplified by 3-kilocycle carrier amplifiers and recorded on an oscillograph. The sharp-leading-edge flat-plate model shown in figure 5 was utilized in the nitrogen-condensation study. The disk rake collector of reference 1 was employed in obtaining the present contamination results.

Typical oscillograph records obtained in the present investigation, illustrating arc-chamber pressure, pitot pressure, and force traces are shown in figure 6. These records demonstrate the fast response of the instrumentation, the low oscillatory level of the traces, the short starting transient time of the tunnel, and resultant comparatively long usable running time.

DATA REDUCTION AND ACCURACY

The initial arc-chamber density was determined from the initial arc-chamber pressure, volume, and ambient temperature. This initial density and the measured values of arc-chamber stagnation pressure and test-section pitot pressure following arc discharge were the basic input data for the real-nitrogen data-reduction program presented in reference 6. This program was written to determine the free-stream, after-shock, and stagnation conditions in the test section at arc-chamber stagnation temperatures from 3000° to 4000° K. Simplifying assumptions that no temperature or density gradients existed in the arc chamber and that all thermodynamic states were in equilibrium were made. The validity of these assumptions is discussed in the appendix along with inaccuracies associated with arc-chamber and test-section pressure instrumentation and employment of the data reduction program of reference 6 at stagnation temperatures less than 3000° K. A "velocity correction" which has been applied to the present data is also discussed in the appendix.

For the most unfavorable conditions, uncertainties involved in the instrumentation and data reduction procedure result in the following maximum probable inaccuracies:

M_1, percent	±2.5
p_1, percent	±7.0
T_1, percent	±9.0
ρ_1, percent	±10.0

The maximum uncertainties in the force and moment coefficients as determined from static calibration of the strain-gage balance are:

C_A	±0.02
C_N	±0.02
C_m	±0.01

RESULTS AND DISCUSSION

Nozzle Axial Surveys With 0.100-Inch-Diameter (2.54-mm) Throat

Lateral pitot pressure and corresponding inviscid core Mach number profiles for a range of axial stations from 116.5 to 146.0 inches (2.96 to 3.71 m)

are presented in figure 7. (See fig. 1 for relative location of axial stations.) The profiles of figure 7 were obtained at stagnation temperatures of approximately 1700° and 2200° K, arc-chamber stagnation pressures ranging from 420 to 720 atmospheres (42.6 to 73 MN/m^2), and a nozzle throat diameter of 0.100 inch (2.54 mm).

In order to determine the inviscid core diameter, the survey rake probes 3 inches (7.62 cm) to either side of the nozzle center line were assumed to lie within the usable test core. An average free-stream Mach number was determined from the pitot pressures of these rake probes, and the inviscid core was defined for values of Mach number not exceeding a ±2.5-percent deviation from this average. The inviscid core diameter was then observed to be approximately 9 to 11 inches (22.9 to 27.9 cm) for the present range of nozzle axial stations tested. There is some indication in figure 7 of the Mach number core diameter increasing between axial station extremes.

In figure 8, the average stagnation-pressure ratio and average Mach number across the inviscid core are presented for axial stations from 116.5 to 150.0 inches (2.96 to 3.81 m) and stagnation temperatures of approximately 1700° and 2200° K. A possible explanation for the difference in stagnation-pressure ratio between the two curves of figure 8(a) is that for the present range of arc-chamber stagnation conditions, an increase in boundary-layer thickness due to increasing stagnation temperatures (from 1700° to 2200° K) predominates over the expected decrease in boundary-layer thickness due to the corresponding increase in arc-chamber stagnation pressure (from approximately 500 to 670 atmospheres (50.7 to 67.95 MN/m^2)). Least-square curves fitted to the data of figure 8(b) indicate a linear increase in Mach number of 0.056 per inch (2.2 per m) with increasing axial station for both stagnation temperatures. The 7.5-percent difference in the free-stream Mach number between the two curves of figure 8(b) is attributed to variation in stagnation temperature and the corresponding variation in stagnation-pressure ratio.

Axial variation of effective-area ratio computed from mass flow considerations is shown in figure 9(a). The data indicate a linear increase of effective-area ratio with increasing axial station. Calculated free-stream pressure variation with axial station is illustrated in figure 9(b). At a stagnation temperature of 1700° K, the slope of the curve is essentially constant over the range of axial stations examined. For a stagnation temperature of 2200° K, the static-pressure ratio at an axial station of 116.5 inches (2.96 m) diverges from the trend established by the remaining data; additional data are required in this region to determine the extent and validity of this divergence.

Effect of Variation in Nozzle Throat Diameter

Lateral pitot pressure and corresponding inviscid core Mach number surveys for a range of nozzle-throat diameters are presented in figure 10 for an axial station of 127.0 inches (3.23 m). The data were obtained for arc-chamber stagnation temperatures of 2200° to 2600° K, stagnation pressures from 480 to

780 atmospheres (48.7 to 79.1 MN/m^2), and nozzle-throat diameters from 0.025 to 0.500 inch (0.635 to 12.7 mm). The inviscid core diameter may be seen in figure 10 to increase from approximately 2 inches (5.08 cm) for a throat diameter of 0.025 inch (0.635 mm) to approximately 14 inches (35.56 cm) for a throat diameter of 0.500 inch (12.7 mm). The previously discussed procedure for defining the inviscid core was not applicable to the results obtained with the 0.025-inch-diameter (0.635-mm) throat, and thus, the Mach number corresponding to the nozzle-center-line pitot pressure was used as the reference. It should be pointed out that the existence of an inviscid core for the 0.025-inch-diameter (0.635-mm) nozzle throat is somewhat questionable, since the pitot-pressure-ratio profile looks suspiciously like pipe flow.

Figure 11 illustrates the variation of the average stagnation-pressure ratio and average Mach number within the inviscid test core with geometric-area ratio. Free-stream Mach numbers of approximately 12 to 26 were experienced for arc-chamber stagnation temperatures of 2200° to 2600° K and stagnation pressures from 480 to 780 atmospheres (48.7 to 79.1 MN/m^2) over the range of nozzle throat diameters examined.

The effective-area ratio is plotted against the geometric-area ratio in figure 12 for the present results along with results from other hotshot facilities (refs. 7 and 8). With the exception of the 0.025-inch-diameter (0.635-mm) nozzle throat $\left(\left(\frac{A}{A^*}\right)_{geometric} = 7.9 \times 10^5\right)$, the effective-area ratio was found to vary from approximately 40 to 80 percent of the geometric-area ratio, the percentage decreasing with decreasing throat diameter as expected.

The variation in measured boundary-layer thickness with geometric-area ratio is illustrated in figure 13 for a Mach number range of 12 to 26 and a Reynolds number range, based on nozzle axial station, of approximately 2×10^6 to 2×10^7. Precise experimental determination of the boundary-layer thickness was not entirely possible due to data scatter and survey-rake-probe spacing of 1 inch (2.54 cm). For values of $\left(\frac{A}{A^*}\right)_{geometric}$ of 7.9×10^3, 3.5×10^3, and 2×10^3 (nozzle-throat diameters of 0.250, 0.375, and 0.500 inch (6.35, 9.52, and 12.7 mm)), which correspond to average free-stream Mach numbers of 14.5, 12.6, and 11.6, respectively, the present data are observed to be in good agreement with the semiempirical findings of reference 9 for prediction of turbulent-boundary-layer thickness. However, a discrepancy exists between the present data and the data of reference 9 for nozzle throat diameters less than 0.250 inch (6.35 mm). This lack of agreement may be due to the fact that semiempirical results of reference 9 were obtained from correlation of shock-tunnel conical nozzle data for a Mach number range of 8 to 16 and a Reynolds number range, based on nozzle axial station, of 1.5×10^5 to 1×10^6, and thus, successful correlation for present Mach numbers greater than 16 (corresponding to nozzle throat diameters less than 0.250 inch (6.35 mm)) is not unexpected. The existence of a laminar nozzle boundary layer due to increasing Mach number and decreasing Reynolds number with decreasing nozzle throat diameter could possibly result in the type of deviation shown in figure 13.

Boundary-layer displacement thicknesses computed from mass flow considerations are shown in figure 14 as a function of geometric-area ratio. Values of displacement thickness derived from the semiempirical and theoretical findings of references 9 to 11 are also presented. The semiempirical relationships of references 9 and 10 were obtained from experimental nozzle (contoured and conical) data, which were correlated in terms of free-stream Mach number and free-stream Reynolds number based on nozzle axial station. As shown in figure 14, the findings of references 9 and 10 are observed to predict the displacement thickness well over the present data regime. Reference 11 predicts the trend but gives values approximately twice those of the present data. The prediction of reference 11 for boundary-layer displacement thickness was not based on experimental data, but was obtained as a correlation factor for displacement thickness computed from numerical integration of the momentum integral equation over a range of Mach numbers from 11 to 19.

In order to remove Mach number dependence from the correlation of boundary-layer displacement thickness, the ratio of boundary-layer displacement thickness to nozzle axial station is expressed (ref. 9) as a function of Reynolds number where density and viscosity are evaluated at the Eckert reference enthalpy defined (ref. 9) as

$$H_r = 0.5\left(H_1 + H_w\right) + 0.22\left(H_{t,1} - H_1\right)$$

For the present test conditions

$$T_r = 0.254T_1 + 0.278T_{t,2} + 133$$

Assuming thermally perfect gas $\left(p_1 = \rho_r R T_r\right)$

$$\left(N_{Re,x}\right)_r = \frac{\rho_r v_1 x}{\mu_r} = \left(1.308 \times 10^5\right) p_1 v_1 x T_r^{-2.5}\left(T_r + 100\right)$$

The correlated boundary-layer displacement thickness as a function of Reynolds number based on the Eckert reference enthalpy is shown in figure 15. The displacement thicknesses for the present investigation were calculated from mass flow considerations and are correlated with the results presented in reference 9, which include a Mach number range of approximately 8 to 16.

The mass flow rate for the various nozzle-throat diameters is presented in figure 16 as a function of elapsed tunnel run time. Figure 16 shows that for a nozzle throat diameter of 0.100 inch (2.54 mm), the mass flow from the arc chamber during the 100-millisecond tunnel run is 12 percent of the initial charge mass and increases to 85 percent for a 0.500-inch-diameter (12.7-mm) throat with a 50-millisecond run time. The large arc-chamber mass loss for throat diameters greater than 0.100 inch (2.54 mm) illustrates the necessity of time correlation between arc-chamber and test-section measurements.

Variations in nozzle throat diameter and arc-chamber stagnation conditions for various programs conducted in the Langley hotshot tunnel have resulted in the Mach number-Reynolds number regime shown in figure 17. Arc-chamber stagnation temperatures of approximately 1200° to 5000° K, stagnation pressures from 100 to 900 atmospheres (10.1 to 91.2 MN/m^2), and nozzle-throat diameters of 0.025 to 0.500 inch (0.635 to 12.7 mm) have resulted in a variation of free-stream Mach number from approximately 11 to 28 and free-stream Reynolds number per foot from approximately 2×10^4 to 2×10^6 (Reynolds number per meter from approximately 6.6×10^4 to 6.6×10^6). Data at lower stagnation temperatures resulting in higher Mach numbers and Reynolds numbers have been obtained, but the findings of reference 12 imply that the flow was condensed. These data are not included in figure 17.

Figure 18 presents the density-altitude—free-stream-velocity regime simulated in the Langley hotshot tunnel, resulting from variation in nozzle-throat diameter and arc-chamber conditions, and representative earth entry trajectories. Stagnation temperatures of 300° to 5000° K gave a free-stream velocity range of approximately 2×10^3 to 12.5×10^3 feet per second (6.1×10^2 to 3.8×10^3 m/sec). The expected condensation flow regime is represented by the darkened area.

Force and Moment Coefficient Comparison

In order to make a comparison of force data obtained in the present facility with data from other hypervelocity facilities, force and moment coefficients were obtained on a cone with a 9° semiapex angle and a bluntness ratio, r_n/r_b, of 0.30 (shown in fig. 4). The results for a range of angle of attack of 0° to 40° are presented in figure 19 and observed to be in good agreement with the 9° blunted-cone data obtained in the AEDC 50-inch and 100-inch hotshot tunnels, having 10° and 8° total-divergence-angle conical nozzles, respectively, and in the Cornell Aeronautical Laboratory 48-inch hypersonic shock tunnel with a contoured nozzle (ref. 13).

Nitrogen Condensation Results

As discussed in reference 14, the free-stream static pressure can be approximated by plotting the flat-plate surface pressure distribution as a function of $X^{-1/2}$ and extrapolating the data linearly to $\lim X^{-1/2} = 0$. With the use of the sharp-leading-edge flat-plate model shown in figure 5, surface pressure distributions were obtained in nitrogen for a range of arc-chamber stagnation temperatures of 1000° to 2400° K, stagnation pressures from 300 to 700 atmospheres (30.4 to 70.9 MN/m^2), and a free-stream Mach number of approximately 21. These surface pressure distributions with variation in free-stream temperature are illustrated in figure 20. The extrapolated free-stream pressure is observed to be in close agreement with calculated free-stream pressure for free-stream temperatures greater than or equal to 19° K, but yields values larger than calculated free-stream pressure for free-stream

temperatures less than 19° K. This effect is better illustrated in figure 21, where the ratio of extrapolated free-stream pressure to calculated free-stream pressure is plotted as a function of free-stream temperature. The rapid increase in pressure ratio from unity indicates that an apparent condensation onset occurs at a free-stream temperature of about 19° K for a free-stream pressure of approximately 0.001 psi $(6.895\ N/m^2)$. As shown in figure 22, this is in good agreement with the condensation results presented in reference 12 for air and in reference 14 where nitrogen was employed as the test gas.

Contamination Results

Relative stream contamination levels were obtained during the present series of tunnel runs by using a rake containing six 1-inch-diameter (2.54-cm) aluminum disks across the core as in reference 1. The mass increase during the shots was averaged for the six disks and plotted in figure 23 against energy into the gas, along with the results from reference 1. The flagged symbols represent contamination levels for which a magnetic coil was used to rotate the arc during discharge (ref. 1). Arc rotation was attained for the run represented by the lower flagged symbol, but insufficient magnetic flux was present for arc rotation for the run represented by the upper point; no further results have been obtained with the coil.

A comparison of the present results with those from reference 1 reveals that, in general, a lower contamination level has been obtained for the newer arc chamber. There have been runs, however, when insulator or seal failure resulted in much higher contamination levels than those shown in figure 23. The aerodynamic data for this type of run are usually discarded.

The present contamination level is apparently low enough that the aerodynamic effects are within the experimental accuracy of the instrumentation; at least, no effects have been determined. Occasionally, however, the test model may be damaged by the impacting of a portion of the diaphragm used to seal the nozzle entrance until flow initiation.

CONCLUSIONS

An experimental investigation to determine the effects of nozzle throat diameter and nozzle axial station on the flow characteristics has been made in the Langley hotshot tunnel. Results of this investigation along with a force comparison and preliminary condensation results have led to the following conclusions:

1. For a 0.100-inch-diameter (2.54-mm) nozzle throat, an axial Mach number gradient of 0.056 per inch (2.2 per meter) was observed for stagnation temperatures of 1700° and 2200° K.

2. Variation in nozzle-throat diameter from 0.025 inch to 0.500 inch (0.635 to 12.7 mm) for stagnation temperatures of 2200° to 2600° K resulted in test-section free-stream Mach numbers of 12 to 26.

3. Boundary-layer-thickness data for nozzle-throat diameters corresponding to free-stream Mach numbers of 11.6, 12.6, and 14.5 were in good agreement with predictions of a semiempirical relationship, whereas a discrepancy was observed for all other nozzle-throat diameters; boundary-layer displacement-thickness data were in close agreement with semiempirical predictions for all nozzle-throat diameters.

4. Force and moment coefficients obtained on a blunted cone with a 9° semiapex angle and a bluntness ratio of 0.3 at a Mach number of 20 were in good agreement with results from other hypervelocity facilities.

5. Preliminary condensation results for nitrogen obtained by utilizing a sharp-leading-edge flat plate showed that the condensation onset occurred at a free-stream temperature of approximately 19° K for a free-stream static pressure of approximately 0.001 psi ($6.895\ N/m^2$); this is in good agreement with condensation results of other facilities employing air and nitrogen as the test medium.

6. Additional tests with the coaxial-electrode arc-chamber configuration have shown a significant decrease in stream contamination level compared with the results for the original arc chamber incorporating opposed electrodes.

Langley Research Center,
National Aeronautics and Space Administration,
Langley Station, Hampton, Va., October 1, 1965.

APPENDIX

DISCUSSION OF ACCURACY OF MEASURED AND CALCULATED FLOW PARAMETERS

Extension of Data Reduction Program

In order to determine free-stream, after-shock, and stagnation conditions in the test section of the Langley hotshot tunnel, the real-nitrogen data-reduction program of reference 6 was employed. This program was written for an arc-chamber stagnation-temperature range of 3000° to 4000° K. Because most of the present data were obtained for stagnation temperatures less than 3000° K, references 15 and 16 were utilized to determine the degree of inaccuracy resulting from the use of the data-reduction program of reference 6 at a stagnation temperature of 1700° K. Reference 15 presents test-section free-stream, after-shock, and stagnation flow parameters for real nitrogen in thermodynamic equilibrium in correction-factor form. The study of reference 15 covered a range of stagnation temperatures from 1000° to 2800° K and stagnation pressures up to 1000 atmospheres $\left(101.3\ MN/m^2\right)$. The percentage differences between the free-stream parameters - Mach number, pressure, temperature, and density - determined from the data-reduction program of reference 6 and the values found by using references 15 and 16 for a stagnation temperature of 1700° K were essentially negligible (less than 1.0 percent).

Arc-Chamber Temperature Gradients

In order to investigate the validity of the assumption that there were no existing temperature or density gradients in the arc chamber, measurements of free-stream velocity were performed in the Langley hotshot tunnel by photographically observing the propagation of disturbances created by spark discharges in the flow stream. These measurements were obtained at stagnation pressures of 480 to 750 atmospheres $\left(48.7\text{ to }76.1\ MN/m^2\right)$ and a Mach number of approximately 20 (nozzle throat diameter of 0.100 inch (2.54 mm)). The results of the velocity measurements revealed that the assumption of uniform temperature in the arc chamber was not valid and could lead to appreciable errors in calculated free-stream density and temperature. As illustrated in figure 24, where ratios of flow parameters corrected by velocity measurements to those uncorrected are plotted as a function of elapsed run time, the validity of the assumption of uniform arc-chamber temperature is observed to improve with elapsed test time. Thus, to improve the quality of the present data, the "velocity correction" factor was applied and an effort was made to utilize data from later times of tunnel runs. Because velocity measurements were performed only for the 0.100-inch (2.54-mm) nozzle-throat diameter, the assumption was made, for the tests with other throat diameters, that at the maximum and minimum values of elapsed run time, the ratios of velocity-corrected parameters to uncorrected parameters were independent of nozzle-throat diameter. Linear interpolations of these ratios, for the flow parameters of interest, were performed between the elapsed-run-time extremes for the various nozzle-throat diameters and were applied to the present data. Because of the increased mass

flow rate experienced for the nozzle-throat diameters greater than 0.100 inch (2.54 mm), as shown in figure 16, this procedure is believed to be conservative, and hence, an overcorrection to the data for these throats is possible.

Vibrational Nonequilibrium

The theoretical work of reference 17, where the nozzle characteristic parameter $\frac{r^* p_{t,1}}{\tan \phi}$ was employed as a correlation parameter for nitrogen vibrational nonequilibrium, illustrates the possible existence of vibrational-nonequilibrium flow for the present arc-chamber stagnation conditions and nozzle geometry. For the most unfavorable present test conditions (nozzle-throat diameter of 0.025 inch (0.635 mm) and stagnation temperature of 2600° K), the findings of reference 17 predict a 14-percent departure of free-stream temperature from its equilibrium value due to vibrational relaxation of the expanding nitrogen flow. The experimental results of reference 18, where studies of nitrogen vibration by the spectrum-line reversal method were performed in a 15° total-angle conical nozzle for a stagnation temperature range of 2800° to 4600° K, showed that vibrational relaxation rates are faster than existing theoretical predictions. Because of the existing uncertainty associated with prediction of vibrational relaxation rates and the suspected low magnitude of correction required for the possible departure of present test-section parameters from vibrational equilibrium, the assumption of vibrational equilibrium was made for the present investigation.

Accuracy

Test-section pressure transducers were calibrated before each tunnel firing in order to compensate for any time-varying characteristics associated with the transducers and amplifiers. Arc-chamber stagnation-pressure measurements and test-section pitot-pressure measurements were accurate to within ±10 percent and ±5 percent, respectively.

For the most unfavorable conditions, uncertainties involved in instrumentation and data-reduction procedure result in the following maximum probable inaccuracies, which are also presented in the section of this paper entitled "Data Reduction and Accuracy":

M_1, percent	±2.5
p_1, percent	±7.0
T_1, percent	±9.0
ρ_1, percent	±10.0

REFERENCES

1. Smith, Fred M.; Harrison, Edwin F.; and Lawing, Pierce L.: Description and Initial Calibration of the Langley Hotshot Tunnel With Some Real-Gas Charts for Nitrogen. NASA TN D-2023, 1963.

2. Mechtly, E. A.: The International System of Units - Physical Constants and Conversion Factors. NASA SP-7012, 1964.

3. Smotherman, W. E.: A Miniature Wafer-Style Pressure Transducer. AEDC-TR-60-11, U.S. Air Force, Oct. 1960.

4. Smotherman, W. E.; and Maddox, W. V.: Variable Reluctance Pressure Transducer Development. AEDC-TDR-63-135, U.S. Air Force, July 1963.

5. Bailey, A. B.; and Boylan, D. E.: Some Experiments on Impact-Pressure Probes in a Low-Density, Hypervelocity Flow. AEDC-TN-61-161 (Contract No. AF 40(600)-800 S/A 24(61-73)), Arnold Eng. Develop. Center, Dec. 1961.

6. Grabau, Martin; Humphrey, Richard L.; and Little, Wanda J.: Determination of Test-Section, After-Shock, and Stagnation Conditions in Hotshot Tunnels Using Real Nitrogen at Temperatures From 3000 to 4000° K. AEDC-TN-61-82, U.S. Air Force, July 1961.

7. Lukasiewicz, J.; Harris, W. G.; Jackson, R.; Van der Bliek, J. A.; and Miller, R. M.: Development of Capacitance and Inductance Driven Hotshot Tunnels. AEDC-TN-60-222 (Contract No. AF 40(600)-800 S/A 11(60-110)), Arnold Eng. Develop. Center, Jan. 1961.

8. Bianchetta, John F.; and Sivier, Kenneth R.: Operating Experience With the MAC Hypervelocity Impulse Tunnel. Advances in Hypervelocity Techniques, Arthur M. Krill, ed., Plenum Press, 1962, pp. 87-128.

9. Burke, Andrew F.: Turbulent Boundary Layers on Highly Cooled Surfaces at High Mach Numbers. Proceedings of Symposium on Aerothermoelasticity. ASD Tech. Rept. 61-645, U.S. Air Force, 1961, pp. 704-741.

10. Lee, John D.: Axisymmetric Nozzles for Hypersonic Flows. Rept. No. TN(ALOSU)459-1 (WADC TN 59-228), Ohio State Univ. Res. Found., June 1959.

11. Enkenhus, K. R.; and Maher, E. F.: The Aerodynamic Design of Axisymmetric Nozzles for High-Temperature Air. NAVWEPS Rept. 7395, U.S. Naval Ord. Lab. (White Oak, Md.), Feb. 5, 1962.

12. Daum, Fred L.: Air Condensation in a Hypersonic Wind Tunnel. AIAA J., vol. 1, no. 5, May 1963, pp. 1043-1046.

13. Edenfield, E. E.: Comparison of Hotshot Tunnel Force, Pressure, Heat-Transfer and Shock Shape Data With Shock Tunnel Data. AEDC-TDR-64-1, U.S. Air Force, Jan. 1964.

14. Griffith, B. J.; Deskins, H. E.; and Little, H. R.: Condensation in Hotshot Tunnels. AEDC-TDR-64-35, U.S. Air Force, Feb. 1964.

15. Clark, Frank L.; and Johnson, Charles B.: Real-Gas Hypersonic-Nozzle Flow Parameters for Nitrogen in Thermodynamic Equilibrium. NASA TN D-2019, 1963.

16. Ames Research Staff: Equations, Tables, and Charts for Compressible Flow. NACA Rept. 1135, 1953. (Supersedes NACA TN 1428.)

17. Erickson, Wayne D.: Vibrational-Nonequilibrium Flow of Nitrogen in Hypersonic Nozzles. NASA TN D-1810, 1963.

18. Hurle, I. R.; Russo, A. L.; and Hall, J. Gordon: Experimental Studies of Vibrational and Dissociative Nonequilibrium in Expanded Gas Flows. [Preprint] 63-439, Am. Inst. Aeron. and Astronautics, Aug. 1963.

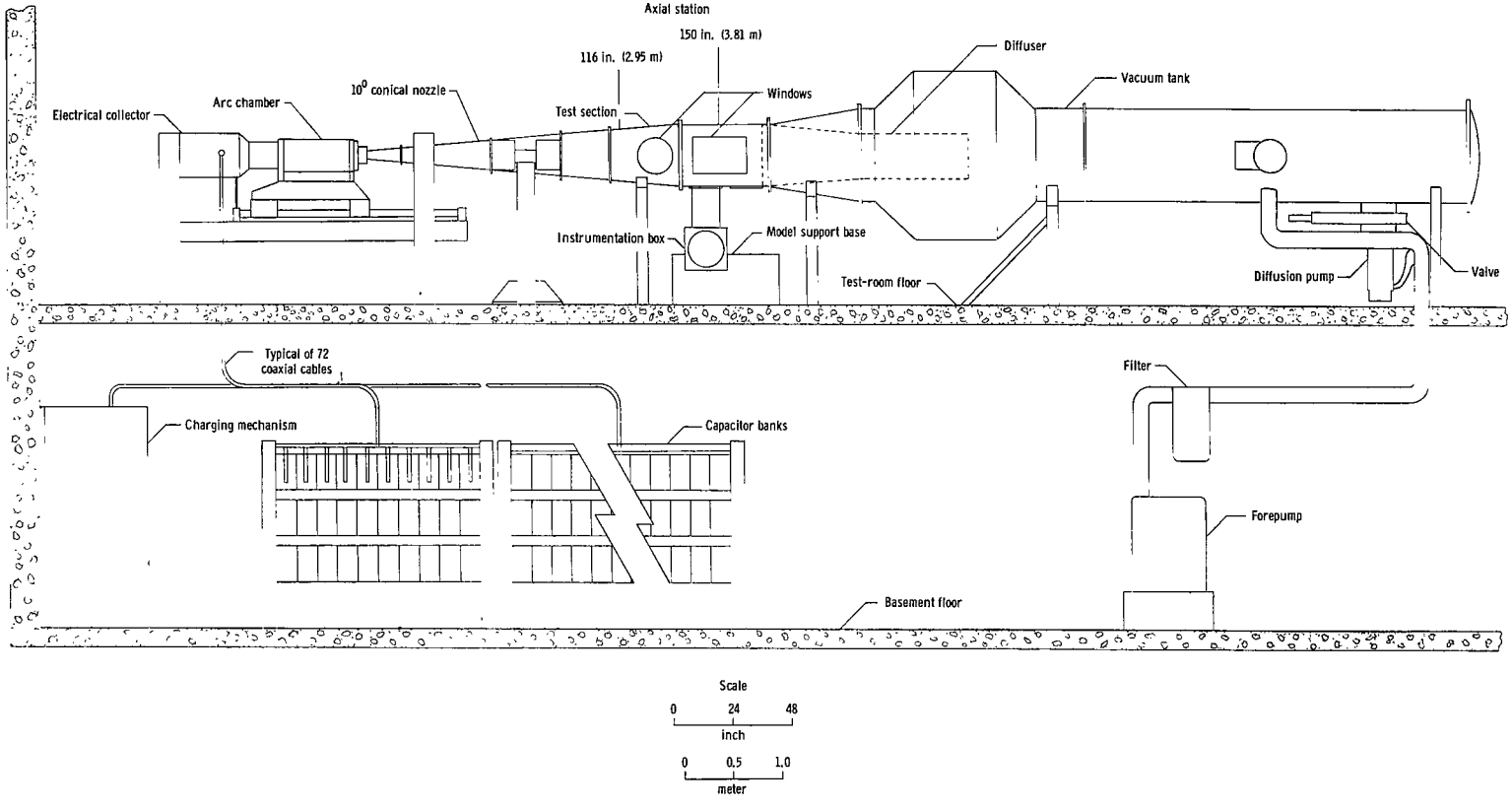

Figure 1.- Elevation view of the Langley hotshot tunnel.

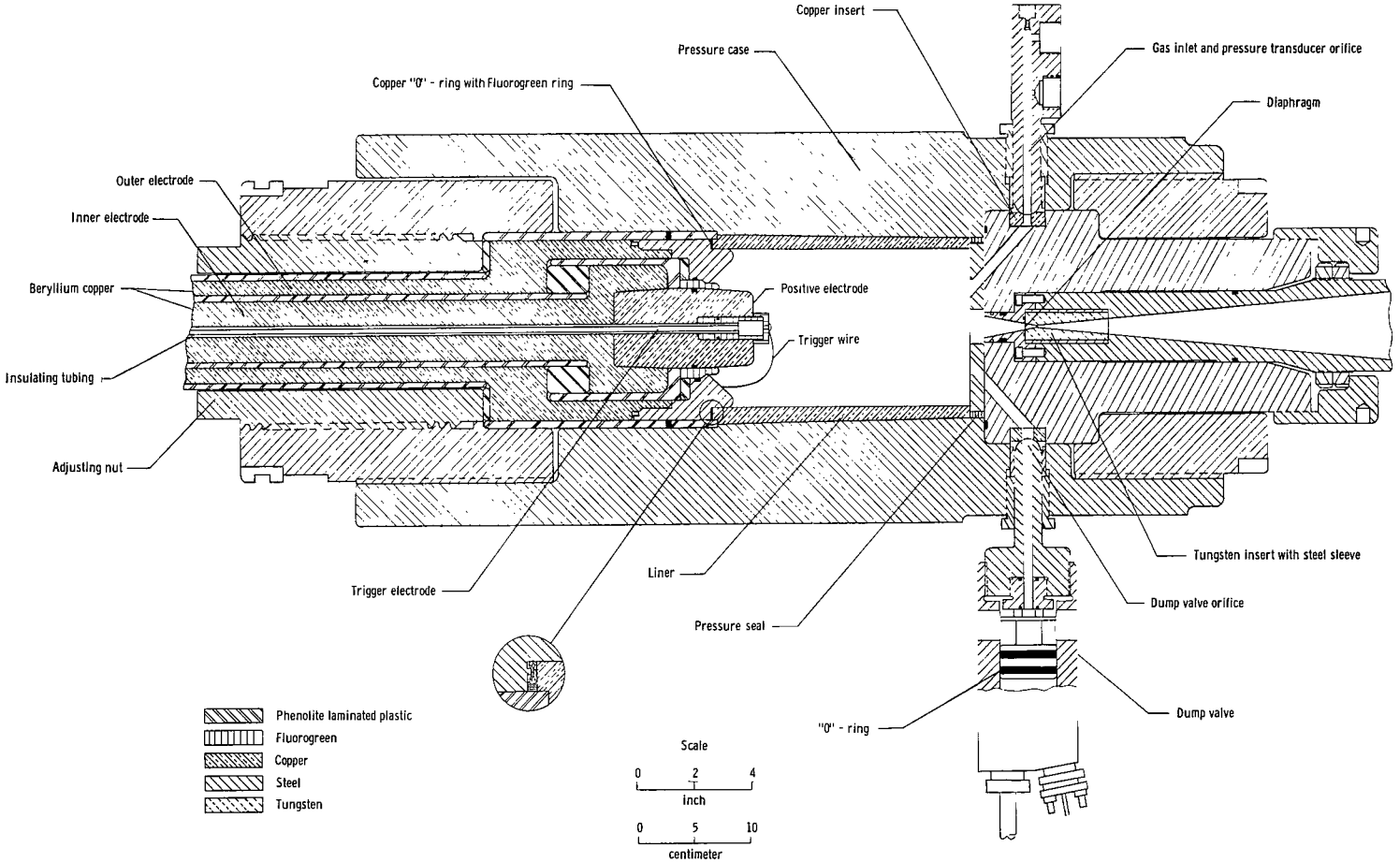

Figure 2.- Arc chamber for the Langley hotshot tunnel.

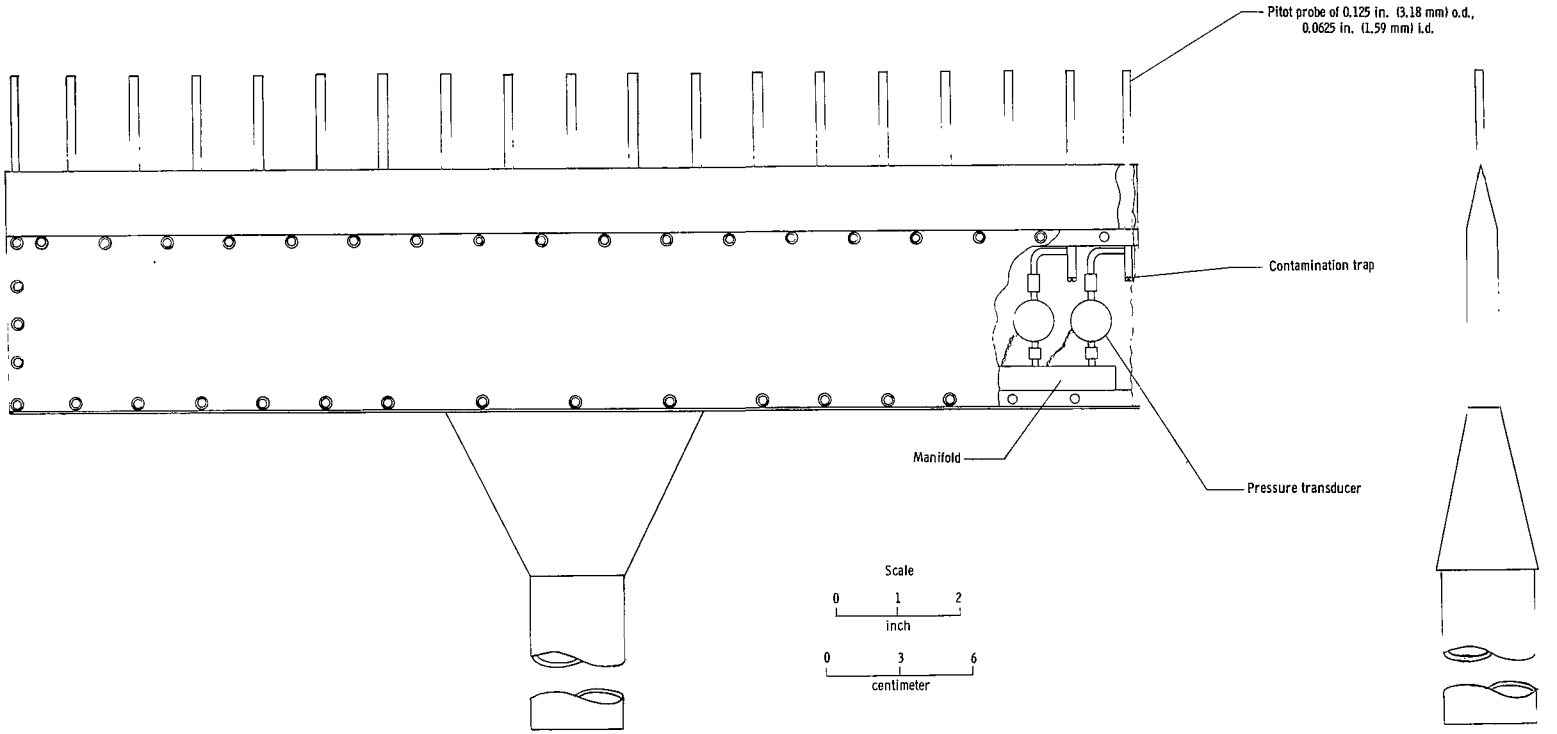

Figure 3.- Pitot-pressure survey rake.

(a) Photograph of force balance. L-63-8155

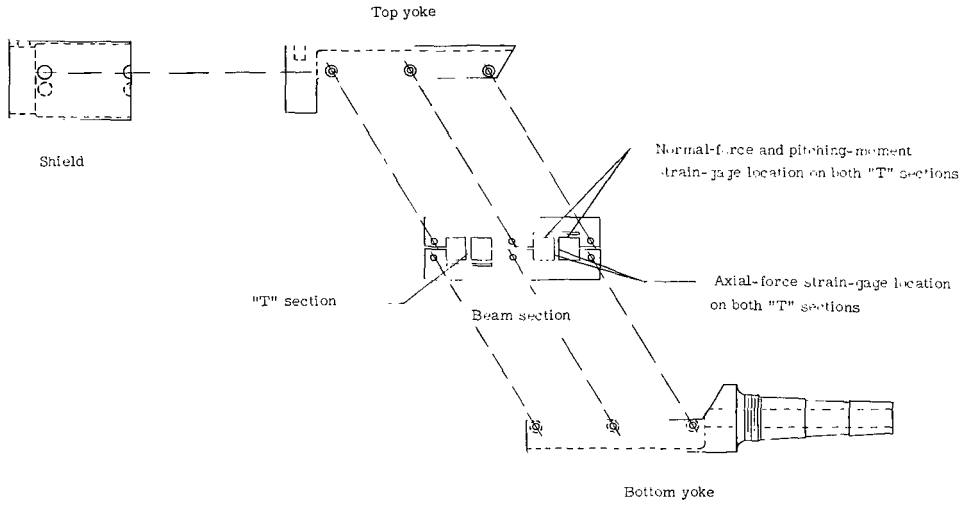

(b) Exploded view of force balance.

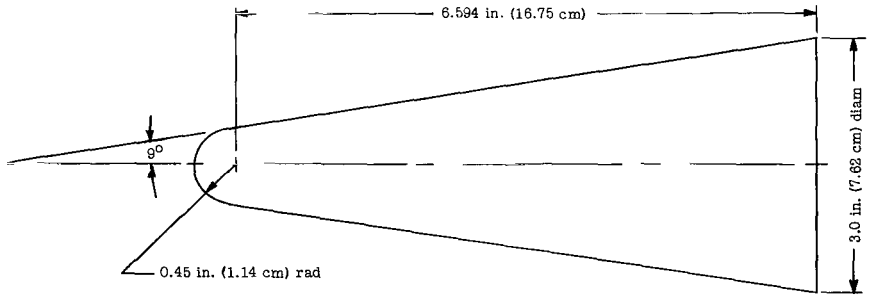

(c) Sketch of force model.

Figure 4.- Force balance and model used in present investigation.

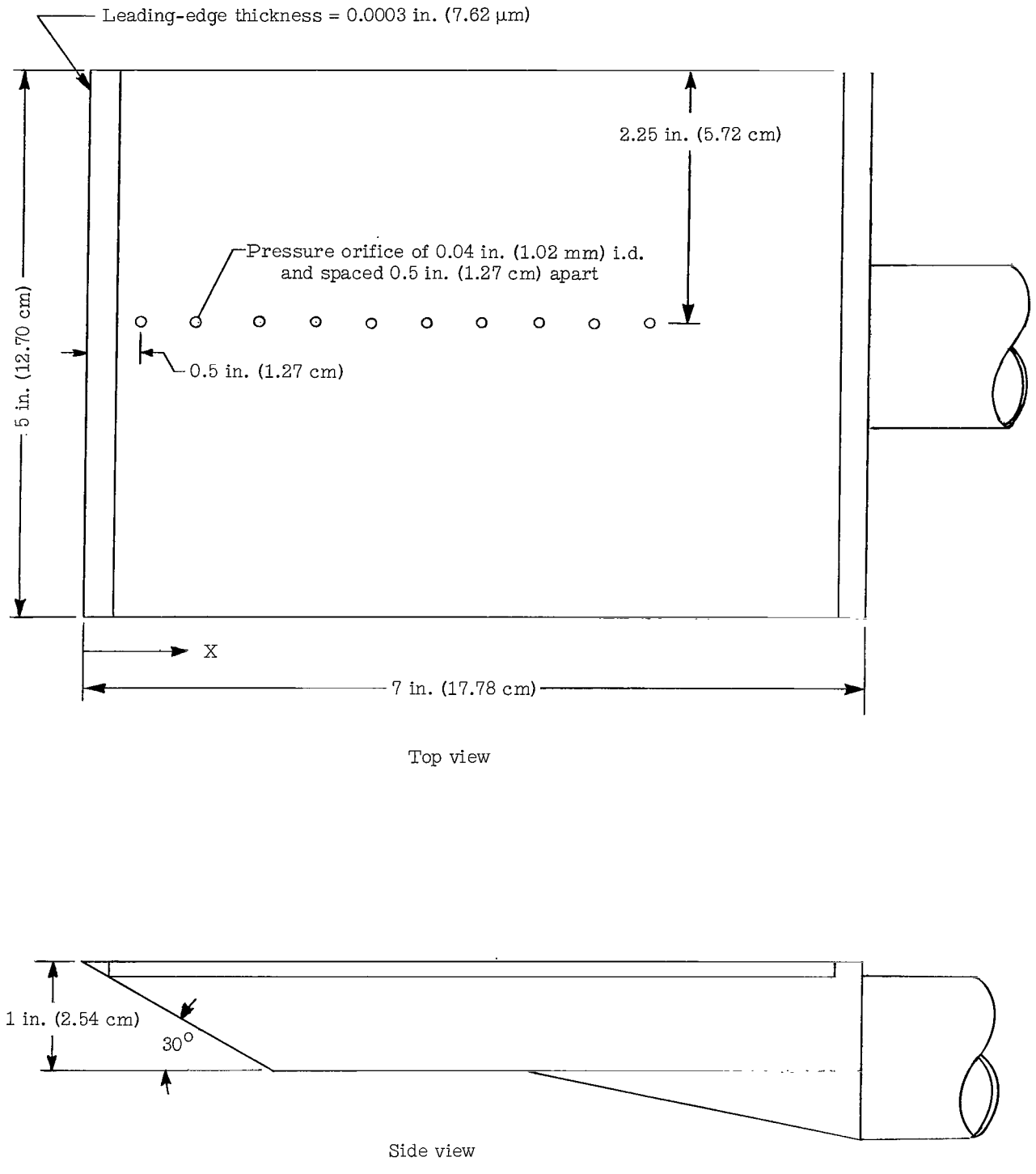

Figure 5.- Flat-plate model employed in the nitrogen condensation study.

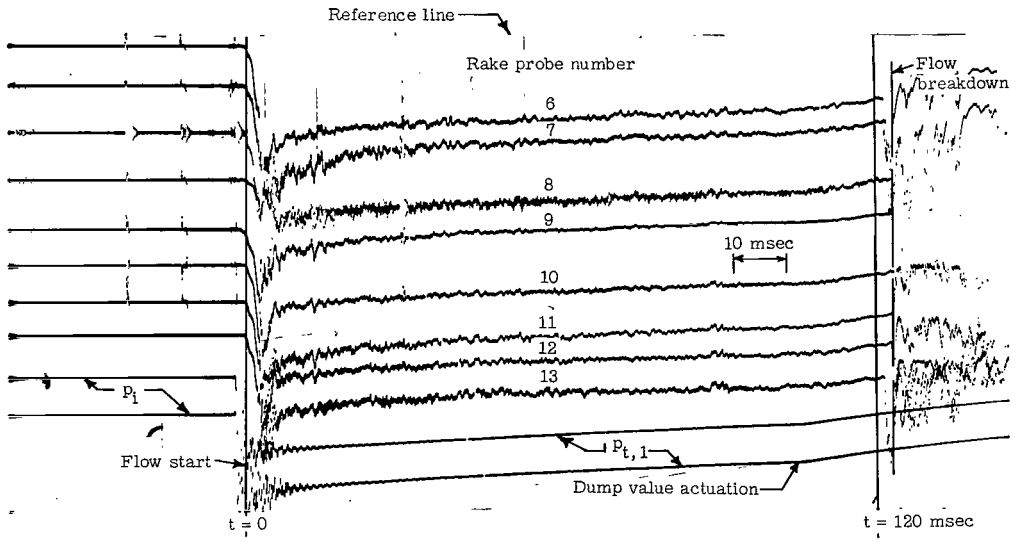

(a) Pressure traces obtained with pitot-pressure survey rake.

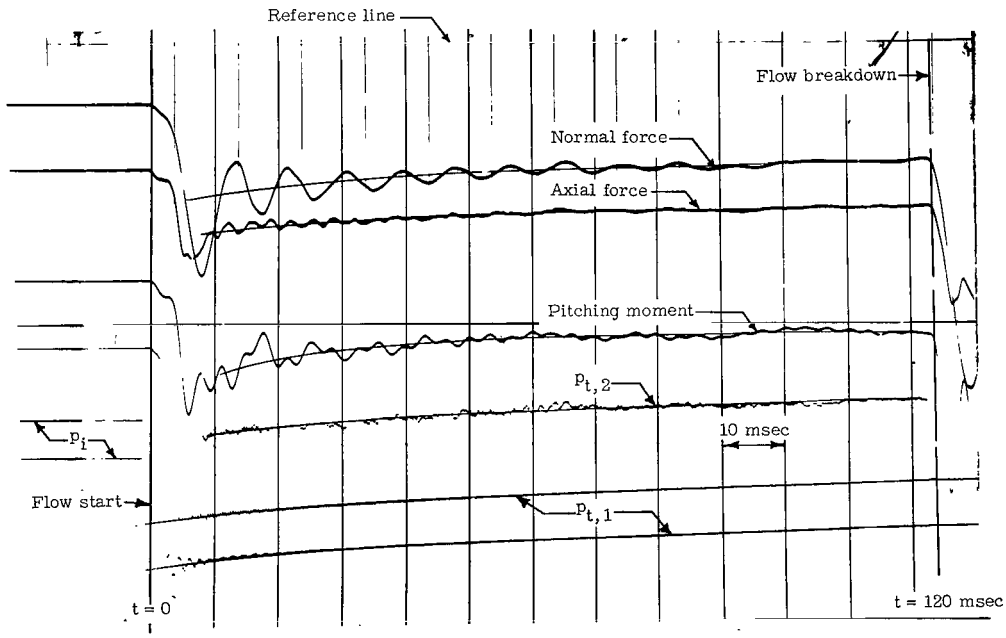

(b) Force traces obtained with blunted cone model. Curves faired through traces for data reduction purposes.

Figure 6.- Representative oscillograph pressure and force records.

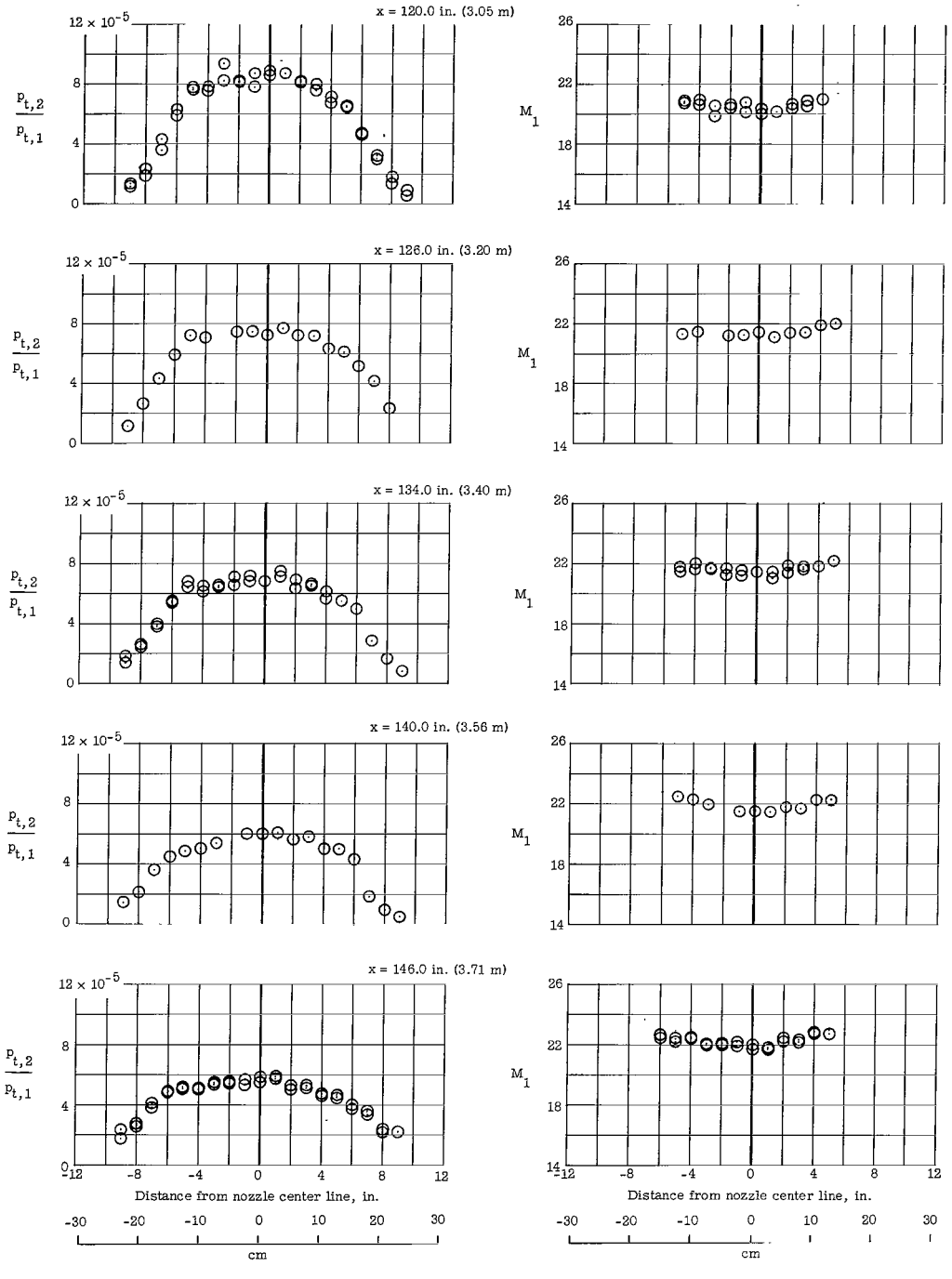

(a) $T_{t,1} \approx 1700^0$ K.

Figure 7.- Representative stagnation-pressure-ratio and Mach number profiles in the test section of the Langley hotshot tunnel for $T_{t,1} \approx 1700^0$ K and 2200^0 K, $p_{t,1}$ = 420 to 720 atm (42.6 to 73.0 MN/m^2), and d* = 0.100 in. (2.54 mm).

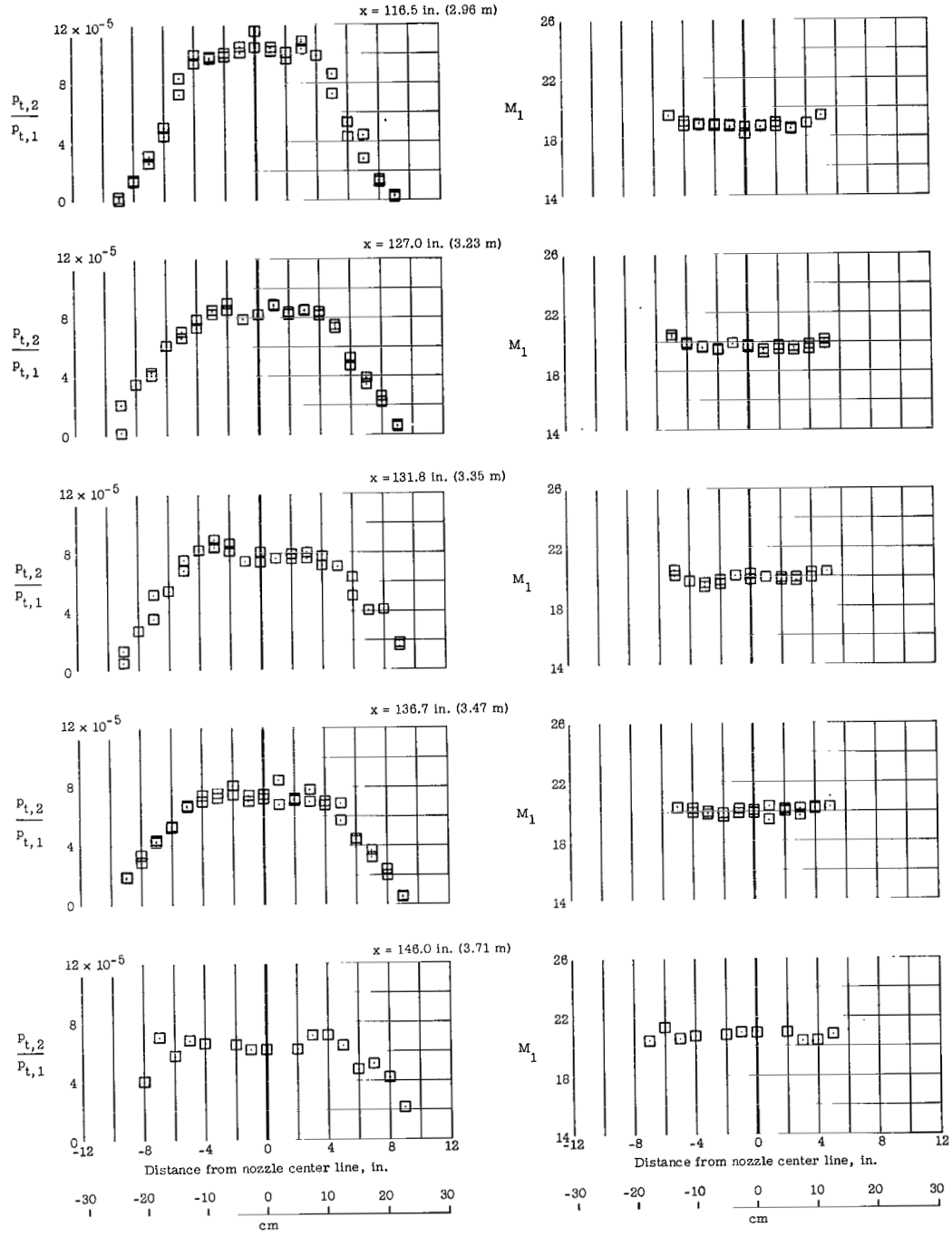

(b) $T_{t,1} \approx 2200^{\circ}$ K.

Figure 7.- Concluded.

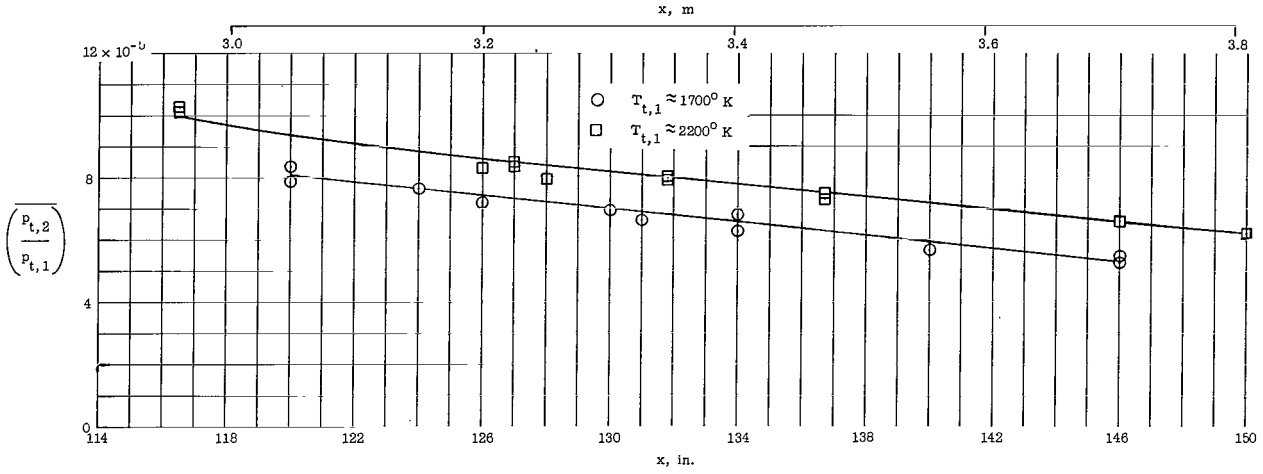

(a) Stagnation-pressure ratio.

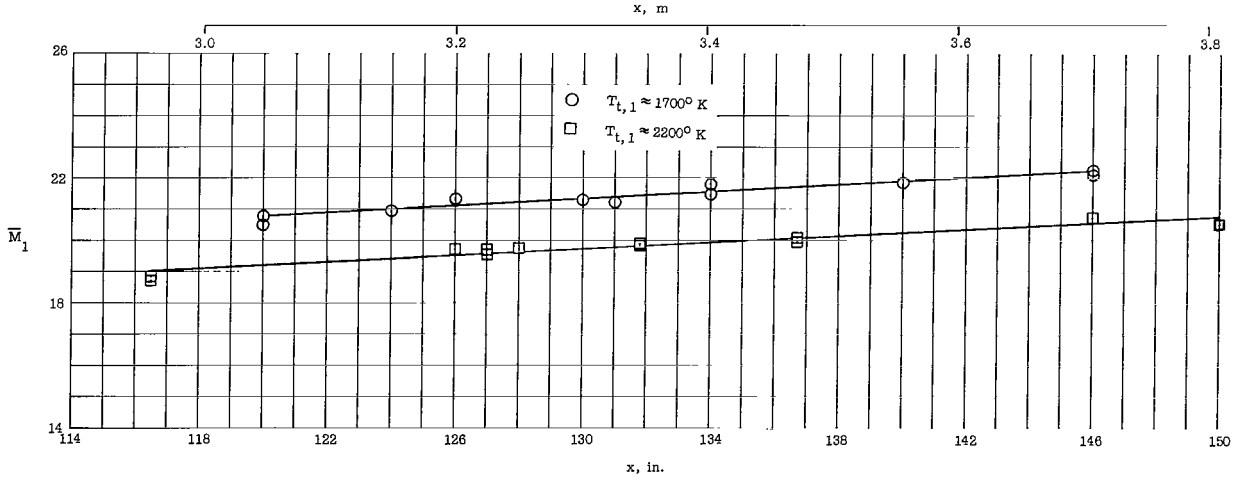

(b) Free-stream Mach number.

Figure 8.- Axial variation of the average stagnation-pressure ratio and Mach number within the inviscid test core. d* = 0.100 in. (2.54 mm).

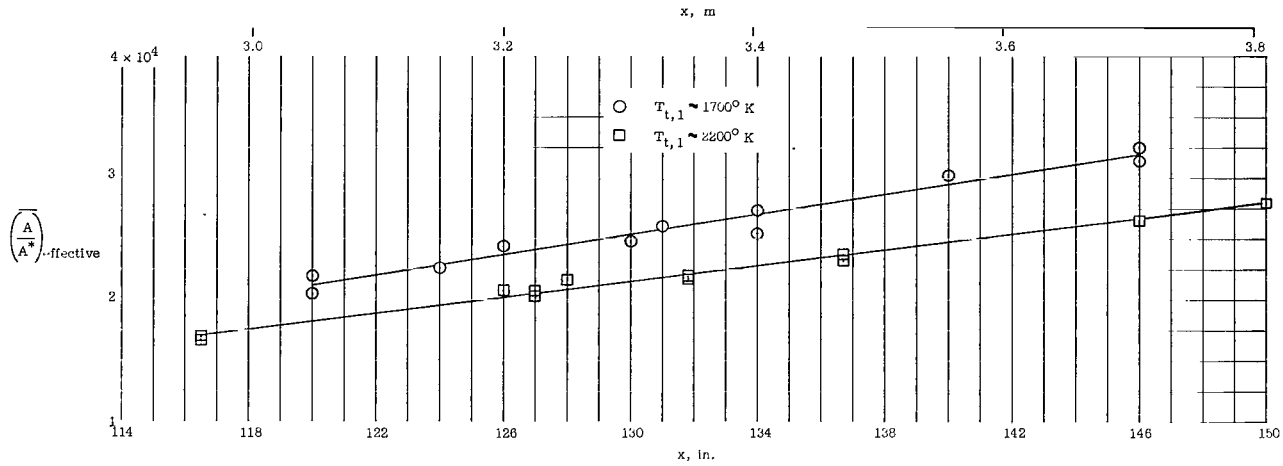

(a) Effective-area ratio.

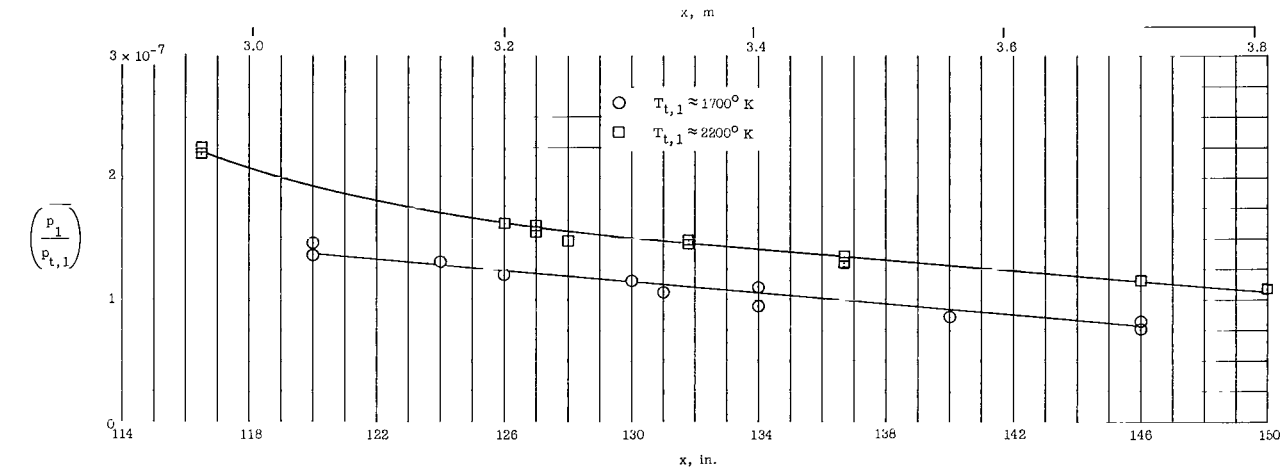

(b) Calculated free-stream static pressure.

Figure 9.- Axial variation of the average effective-area ratio and calculated free-stream static pressure within the inviscid test core. d* = 0.100 in. (2.54 mm).

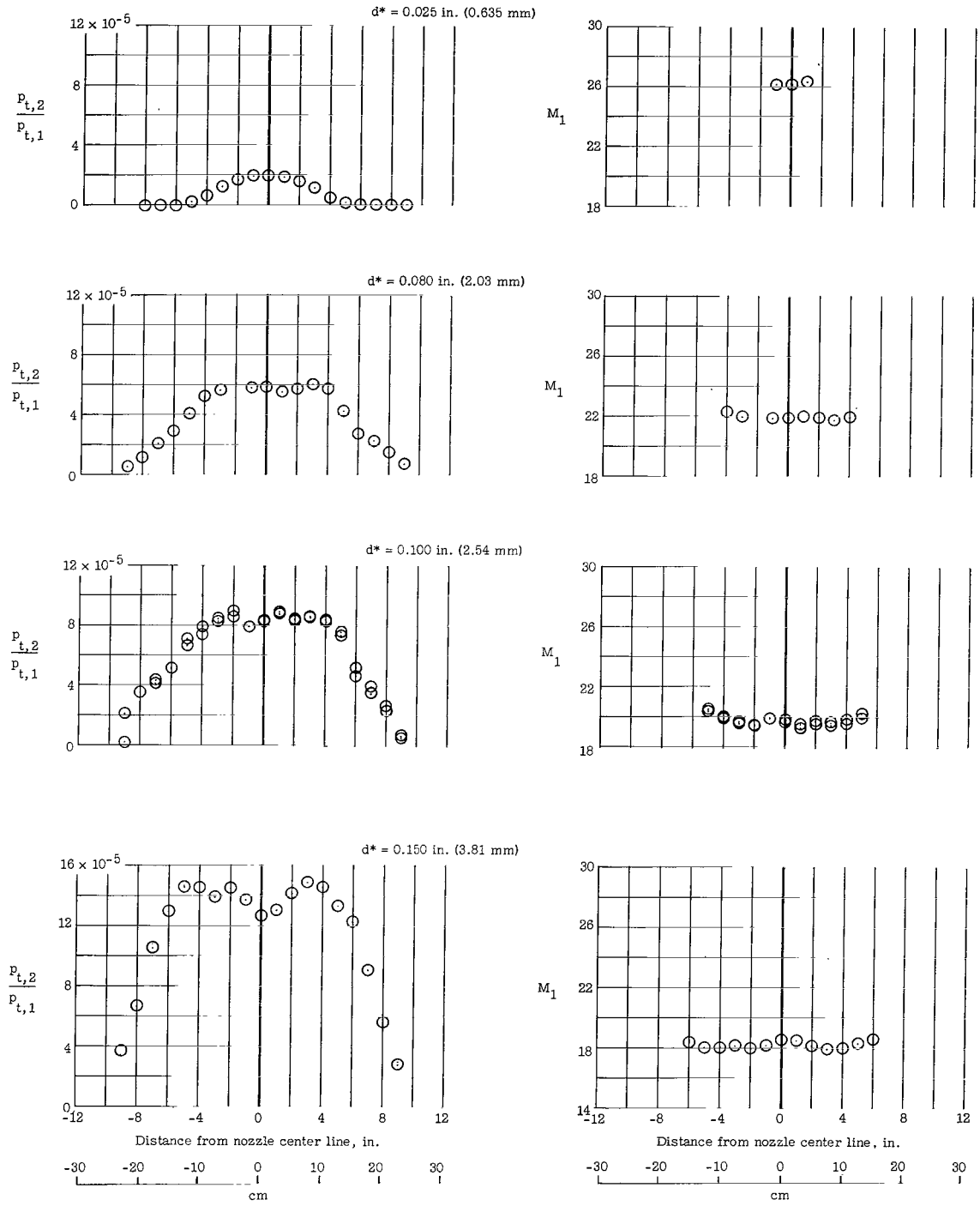

Figure 10.- Stagnation-pressure-ratio and Mach number profiles for various nozzle-throat diameters. $T_{t,1}$ = 2200° to 2600° K; $p_{t,1}$ = 480 to 780 atm (48.7 to 79.1 MN/m^2); x = 127.0 in. (3.23 m).

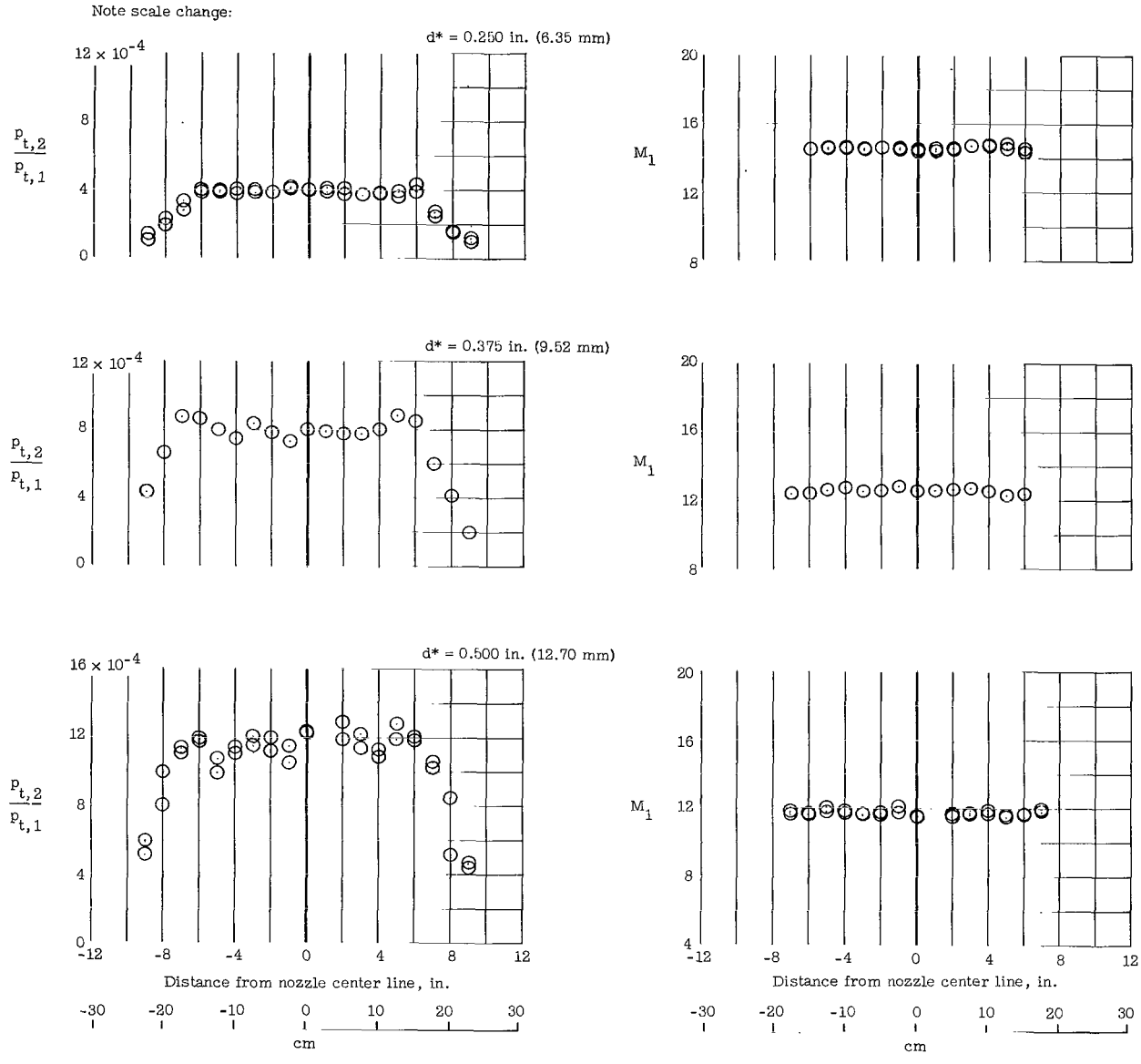

Figure 10.- Concluded.

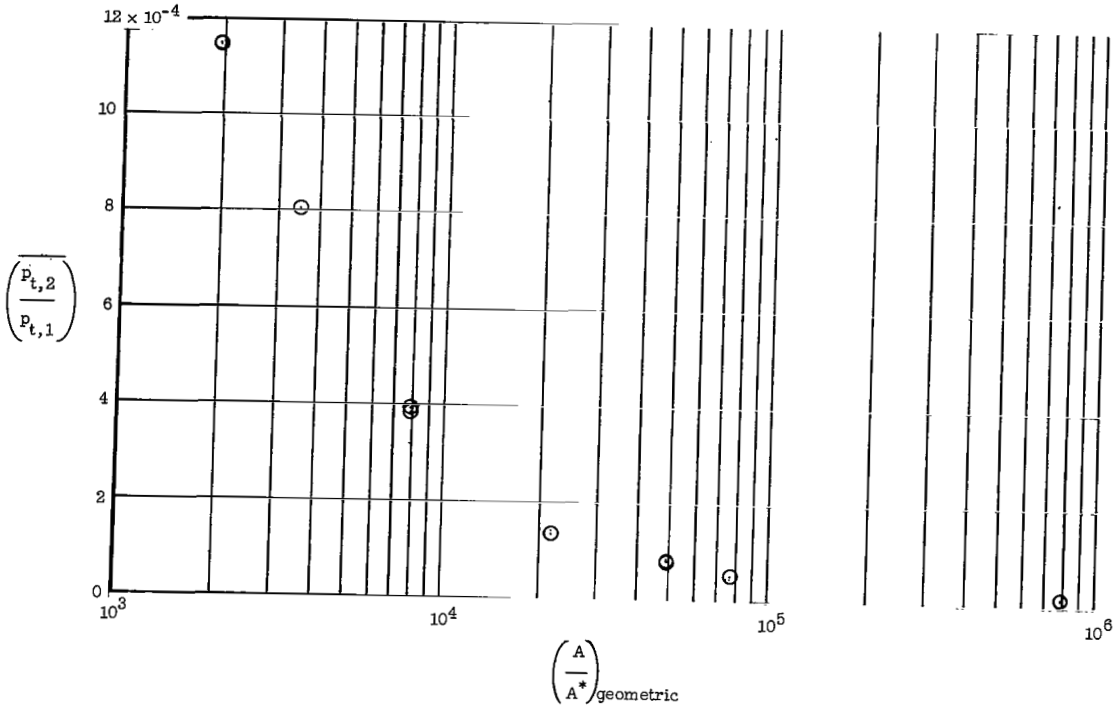

(a) Stagnation-pressure ratio.

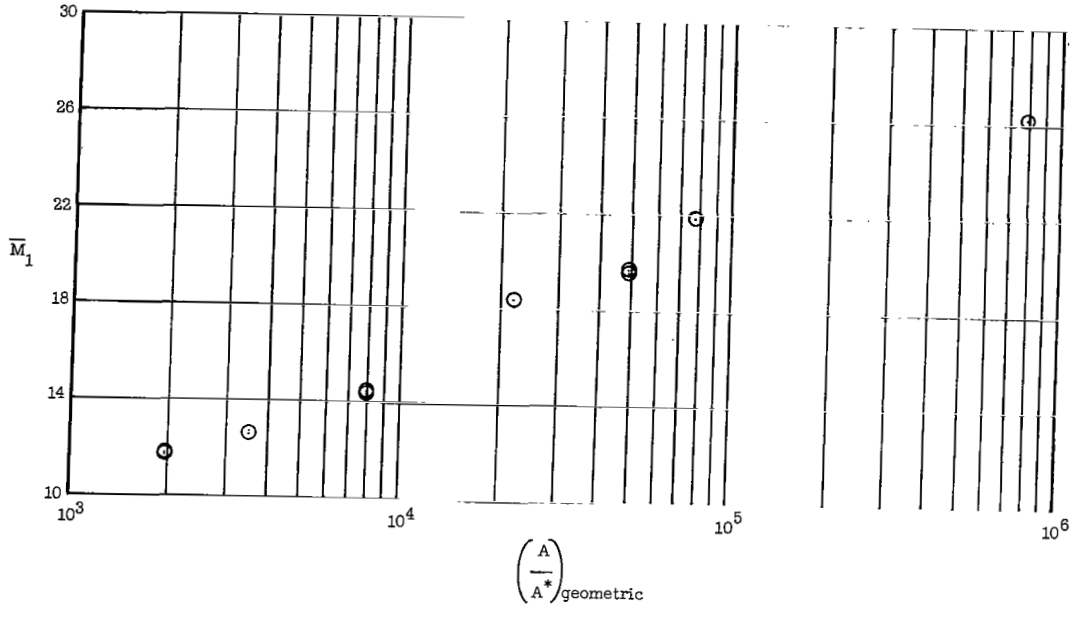

(b) Free-stream Mach number.

Figure 11.- Average stagnation-pressure ratio and Mach number within the inviscid test core as a function of geometric-area ratio. $T_{t,1}$ = 2200° to 2600° K; $p_{t,1}$ = 480 to 780 atm (48.7 to 79.1 MN/m²); x = 127.0 in. (3.23 m).

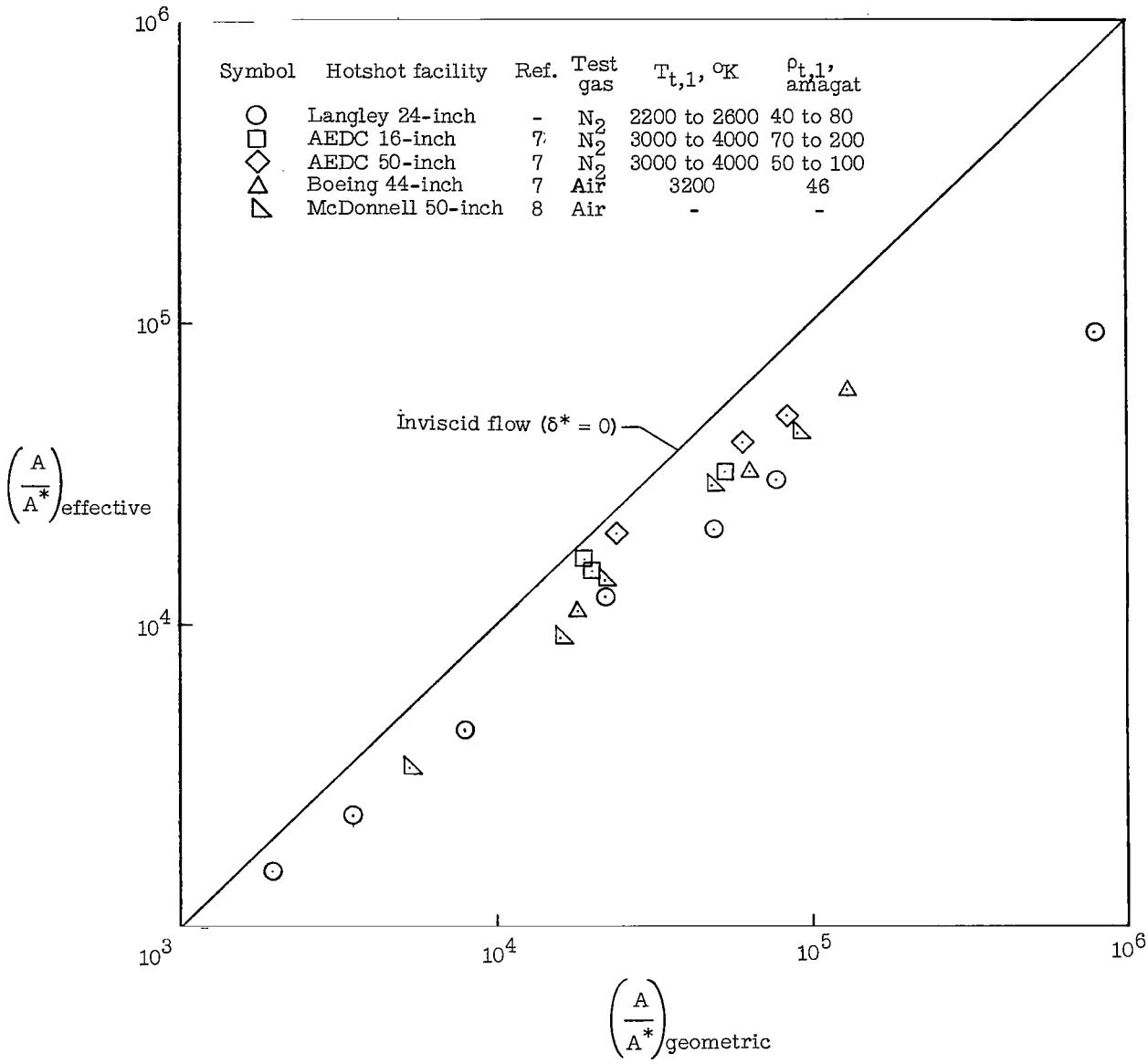

Figure 12.- Variation of effective-area ratio with geometric-area ratio.

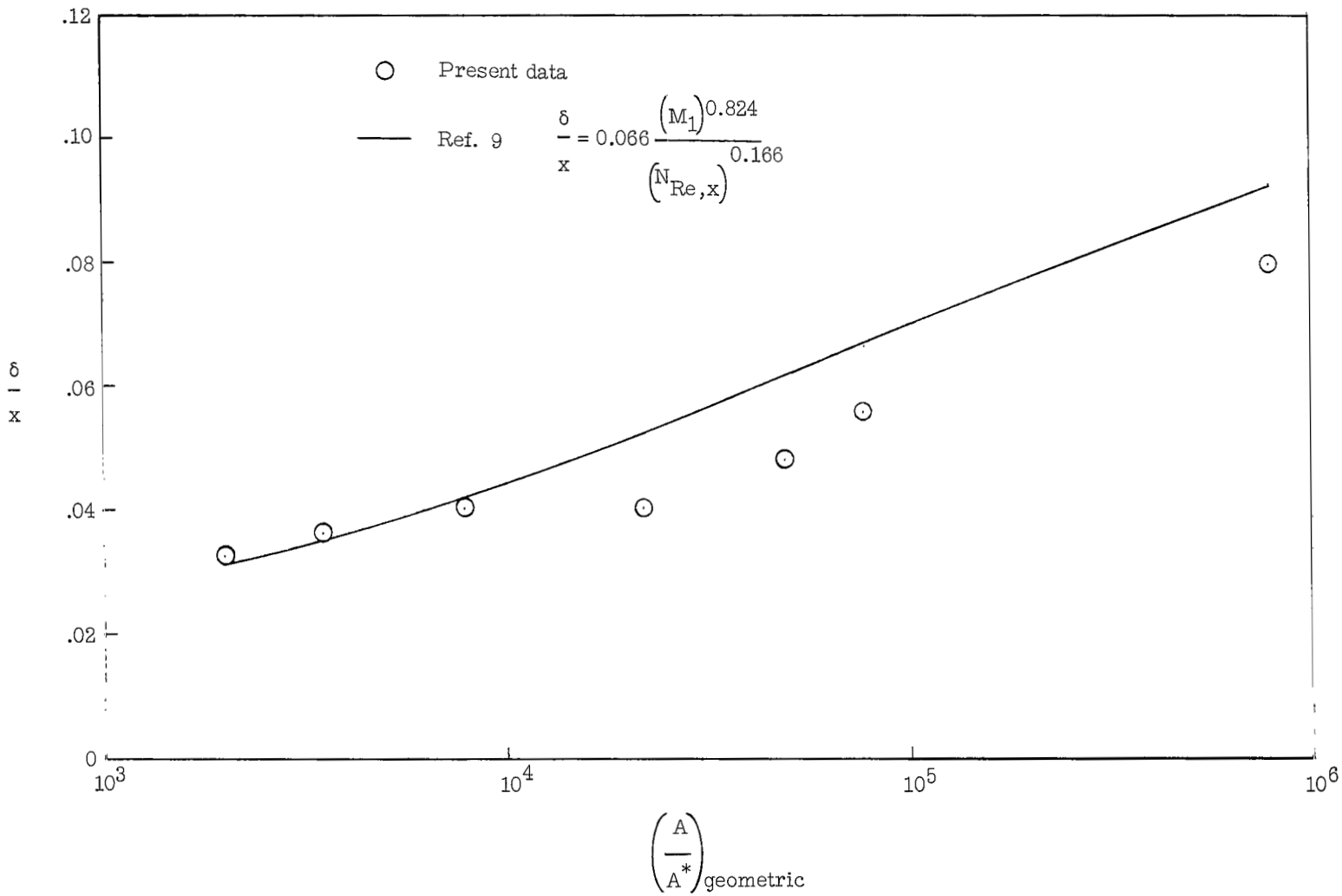

Figure 13.- Variation of boundary-layer thickness with geometric-area ratio.

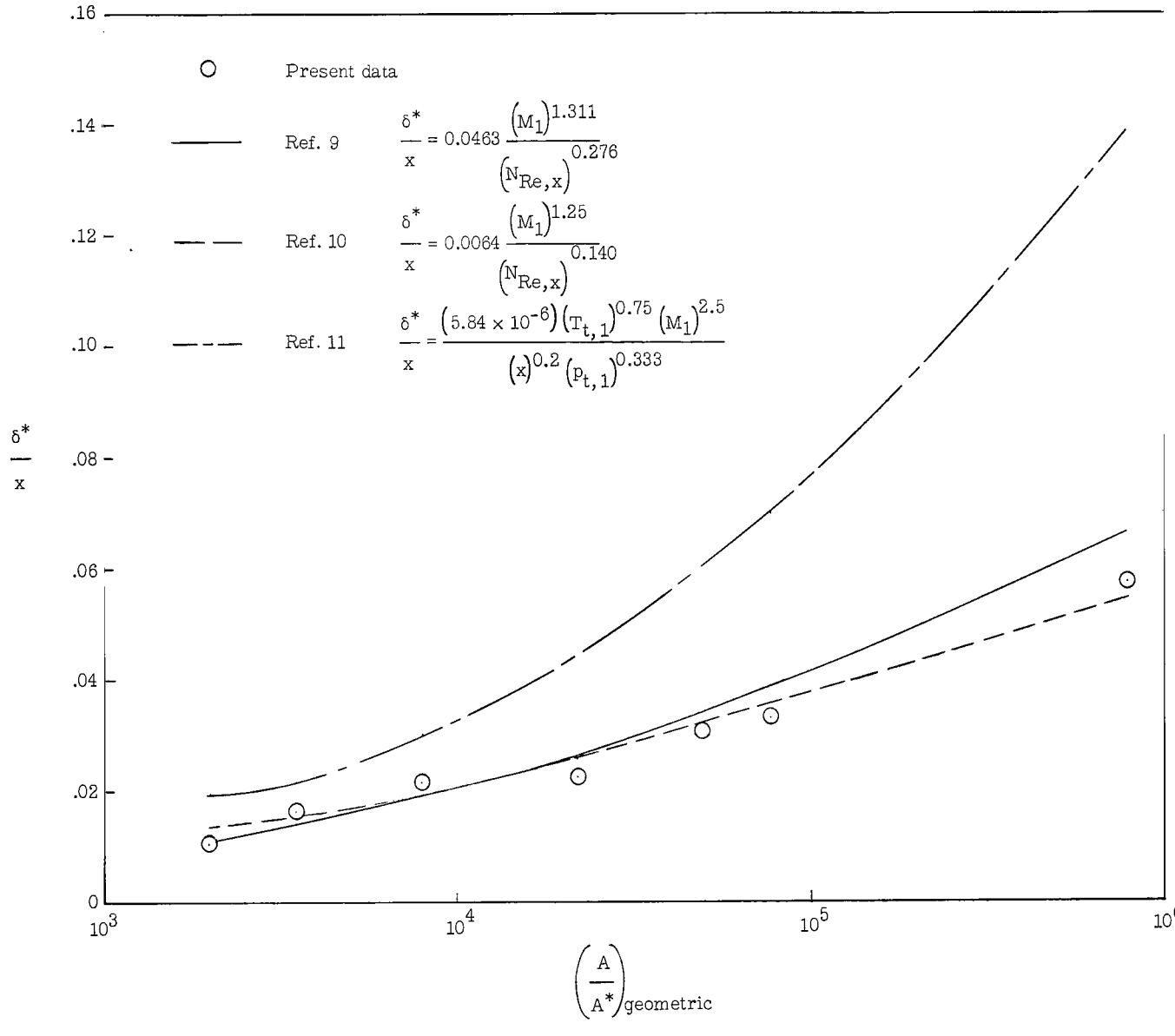

Figure 14.- Variation of boundary-layer displacement thickness with geometric-area ratio.

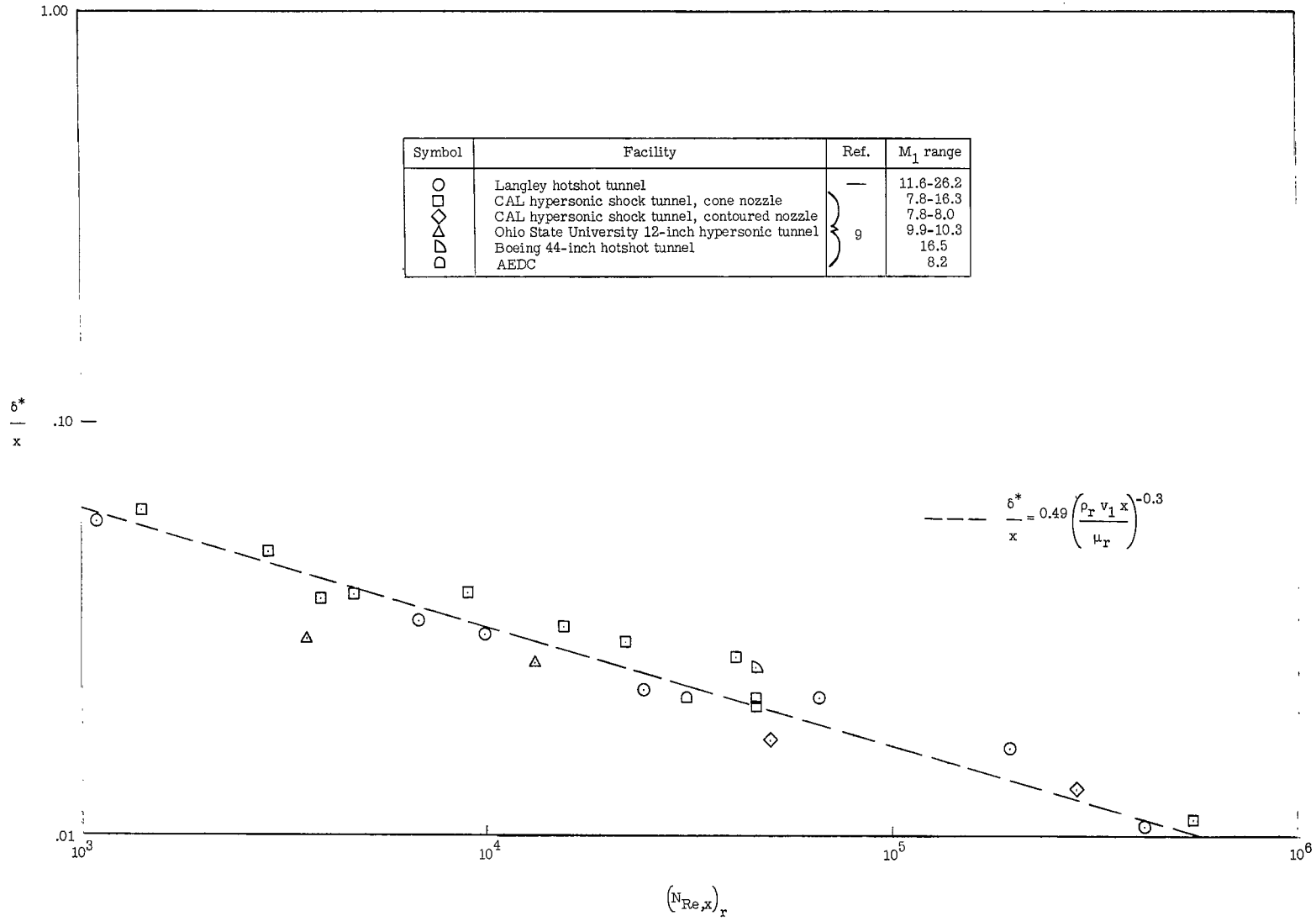

Figure 15.- Boundary-layer displacement thickness correlated in terms of Reynolds number based on the Eckert reference enthalpy.

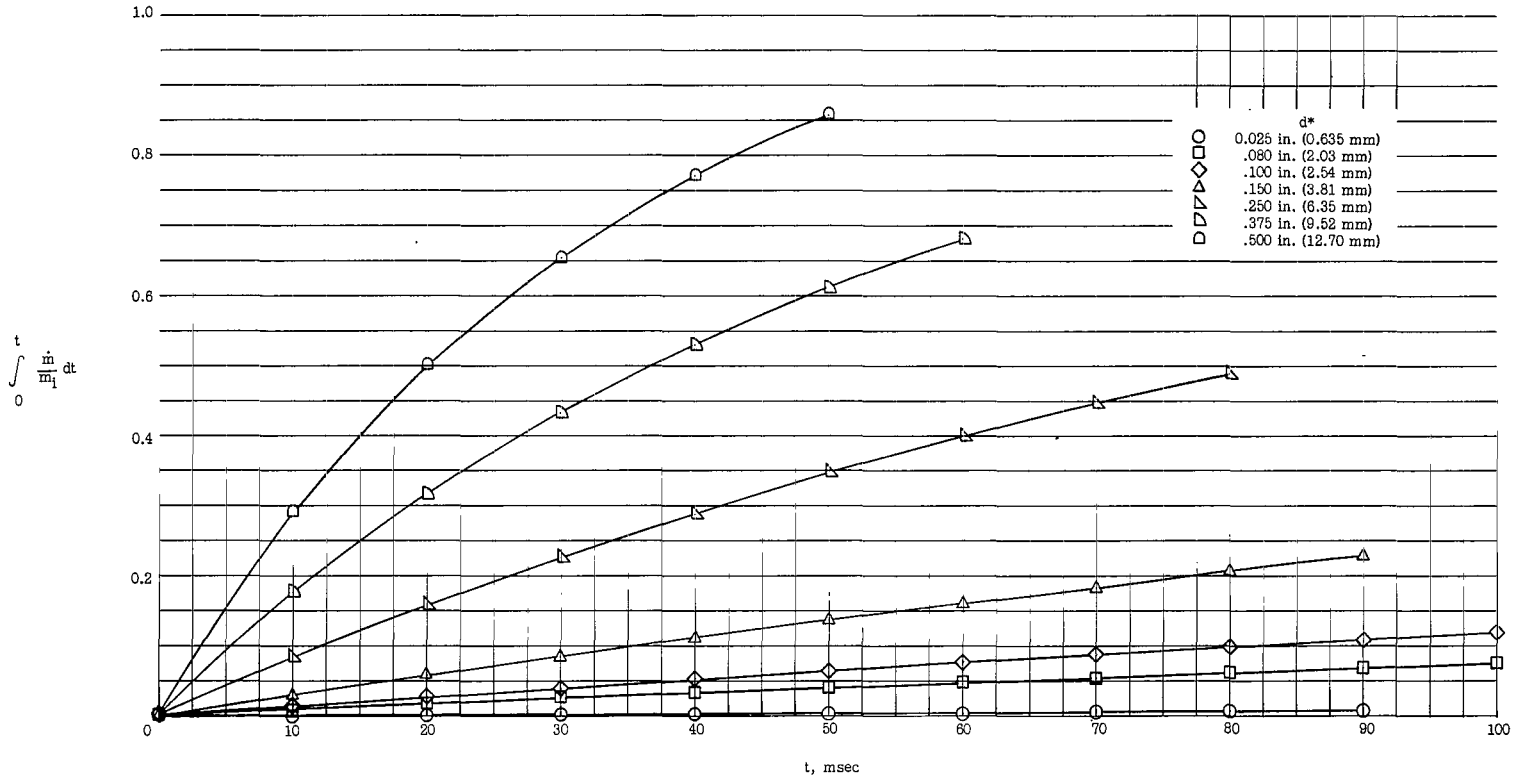

Figure 16.- Ratio of mass flow from arc chamber to initial mass as a function of elapsed run time for various nozzle-throat diameters.

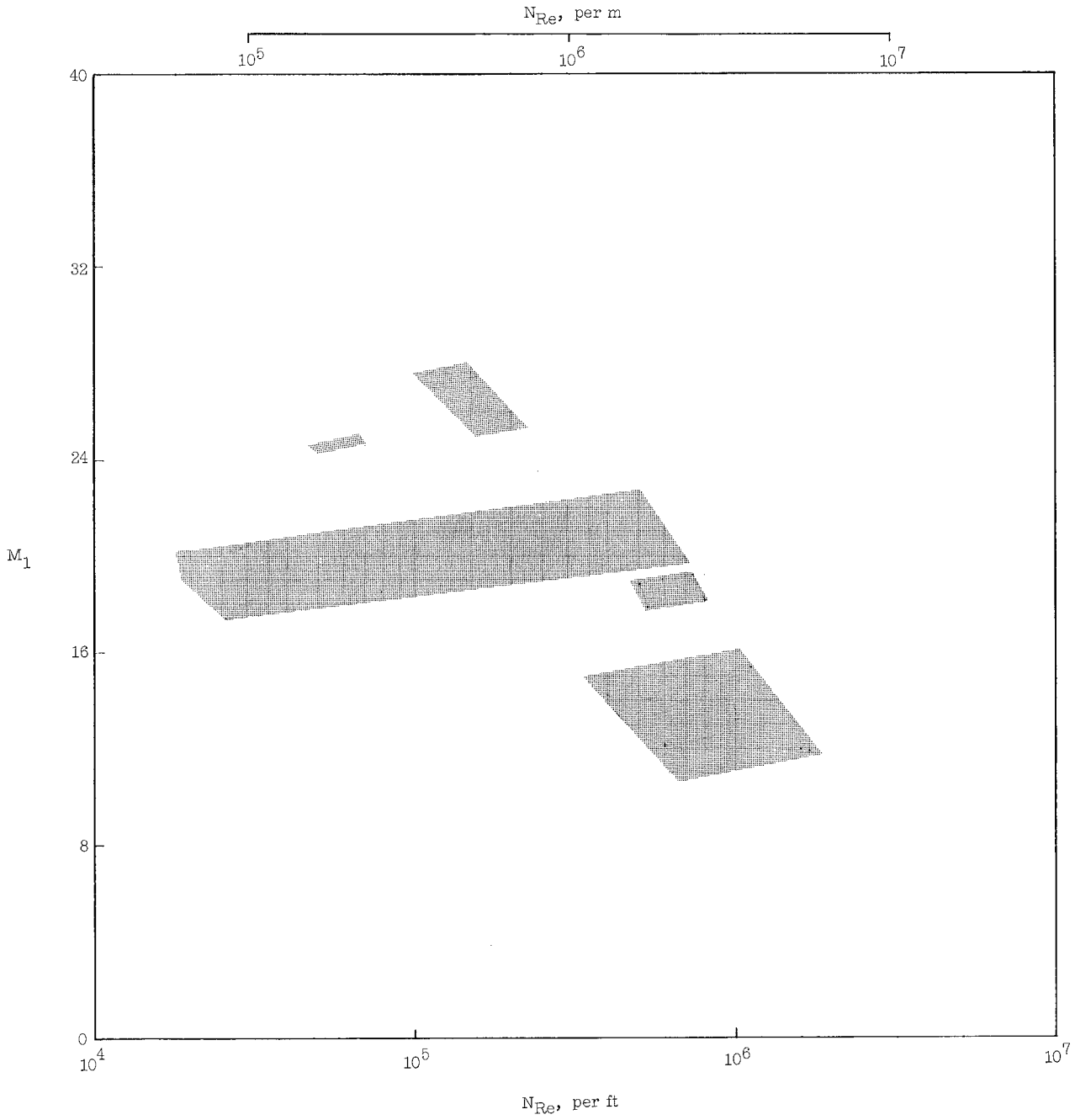

Figure 17.- Condensation-free Mach number-Reynolds number test experience in the Langley hotshot tunnel.

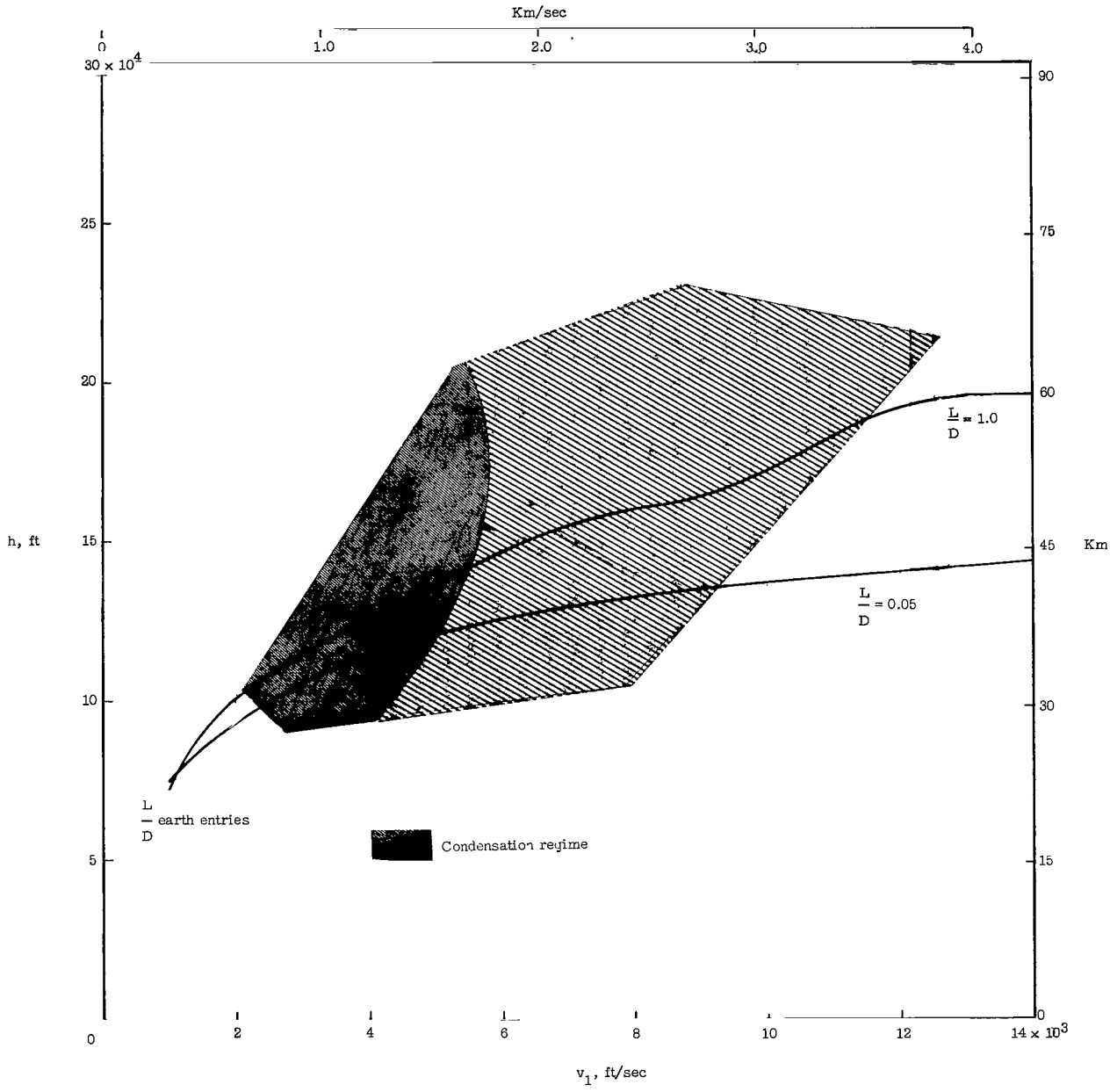

Figure 18.- Density-altitude—velocity test experience in the Langley hotshot tunnel.

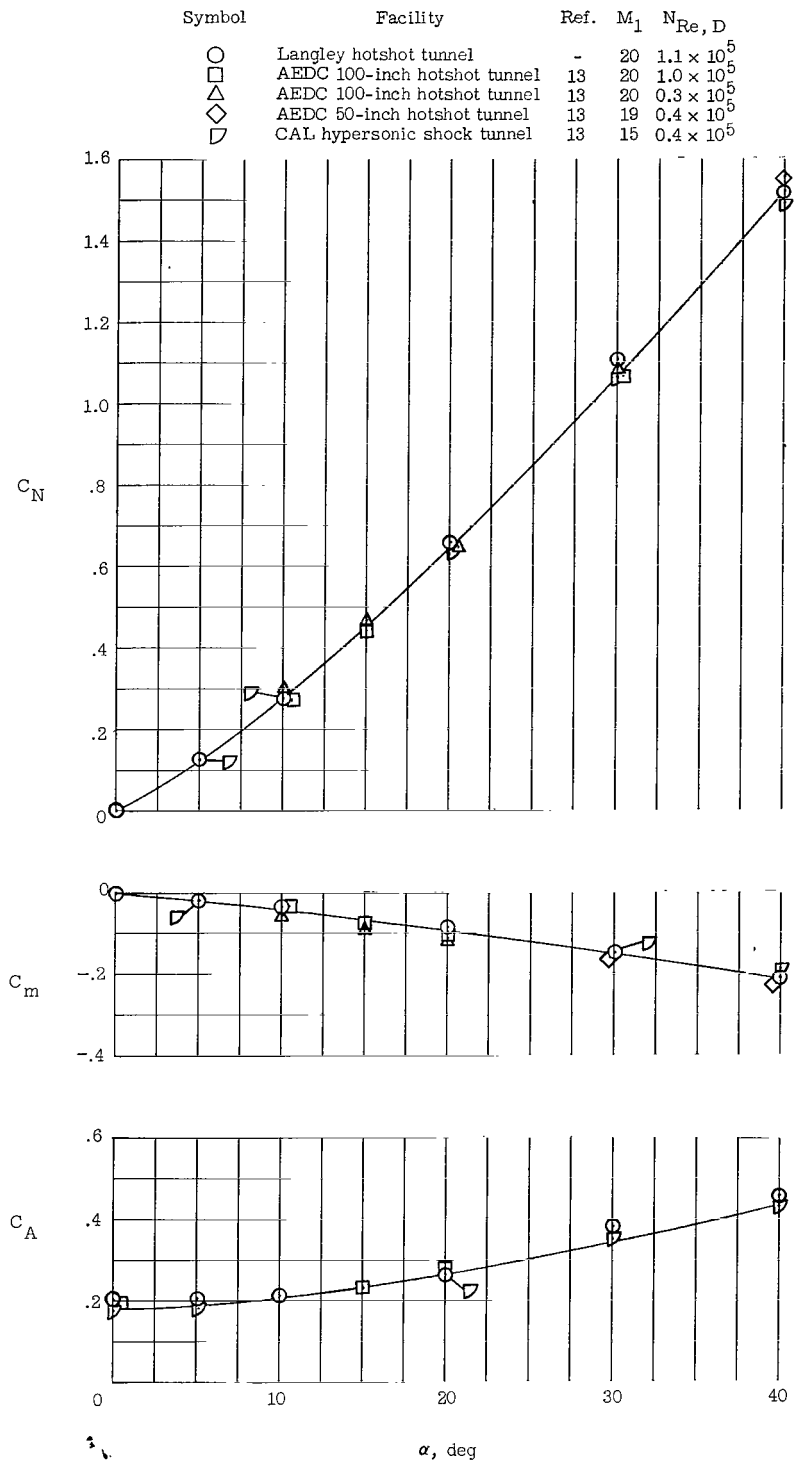

Figure 19.- Force and moment data for 9^0 blunted cone. $\psi = 0.3$.

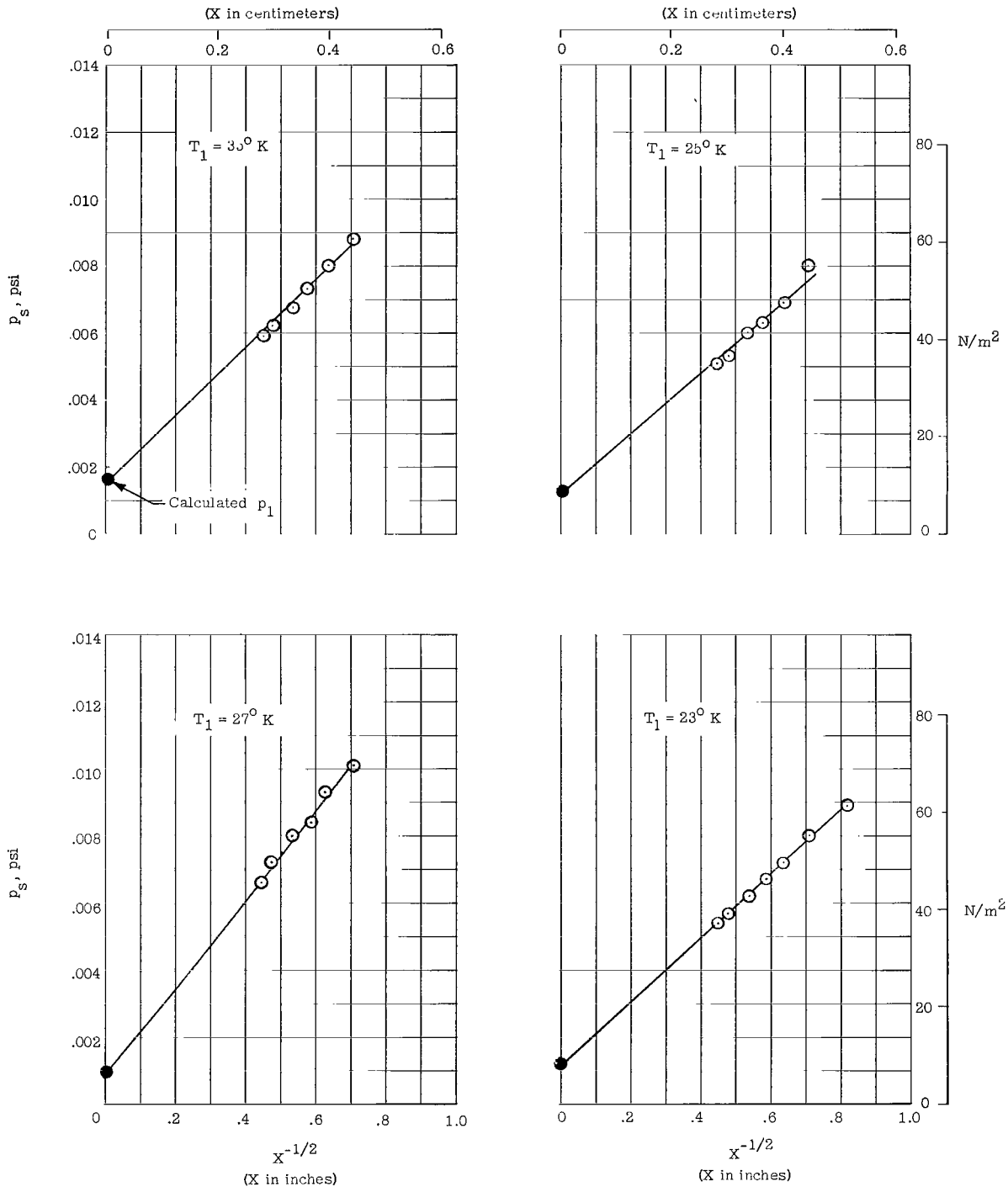

Figure 20.- Flat-plate surface pressure distribution for various free-stream temperatures and $M_1 \approx 21$.

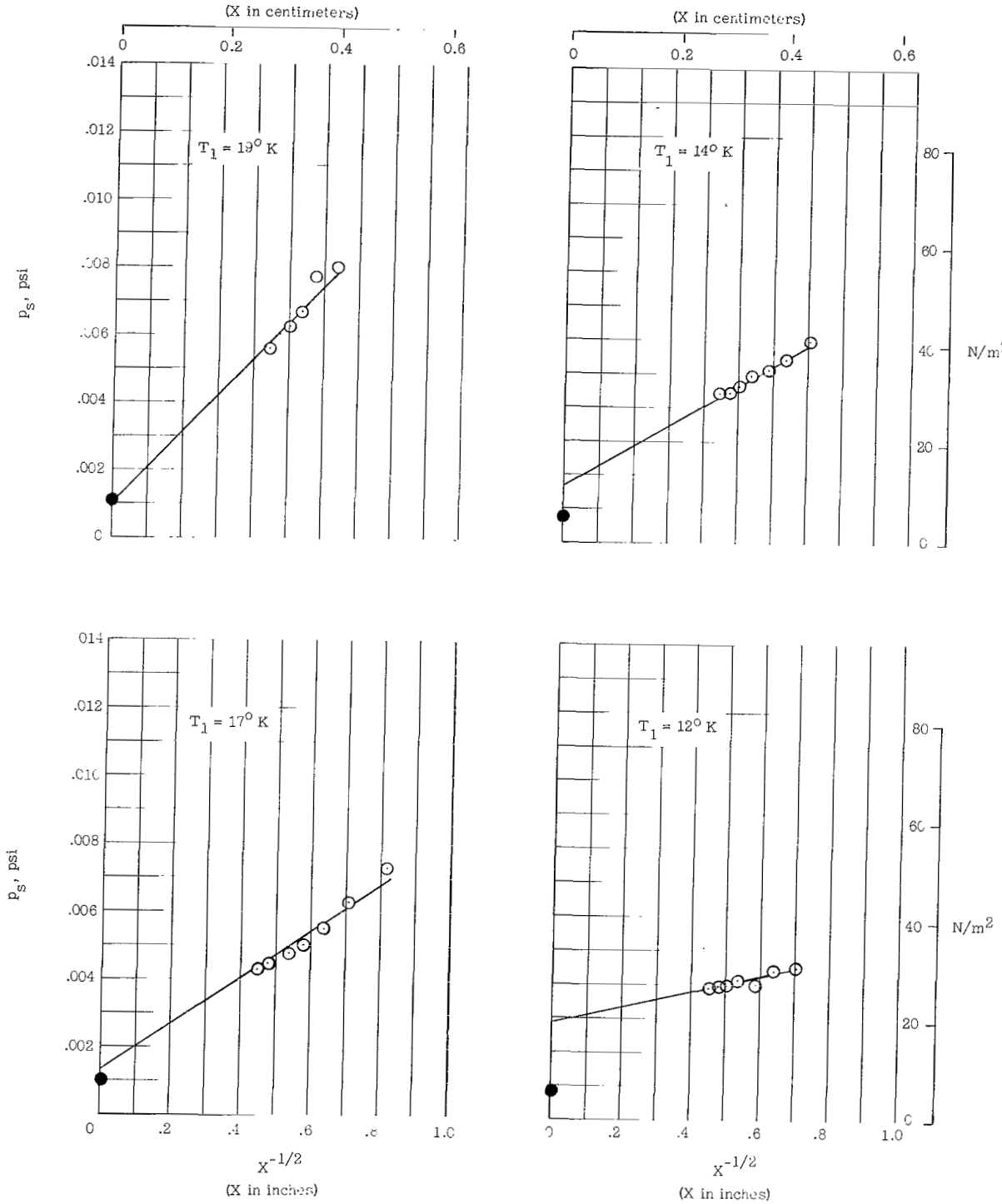

Figure 20.- Concluded.

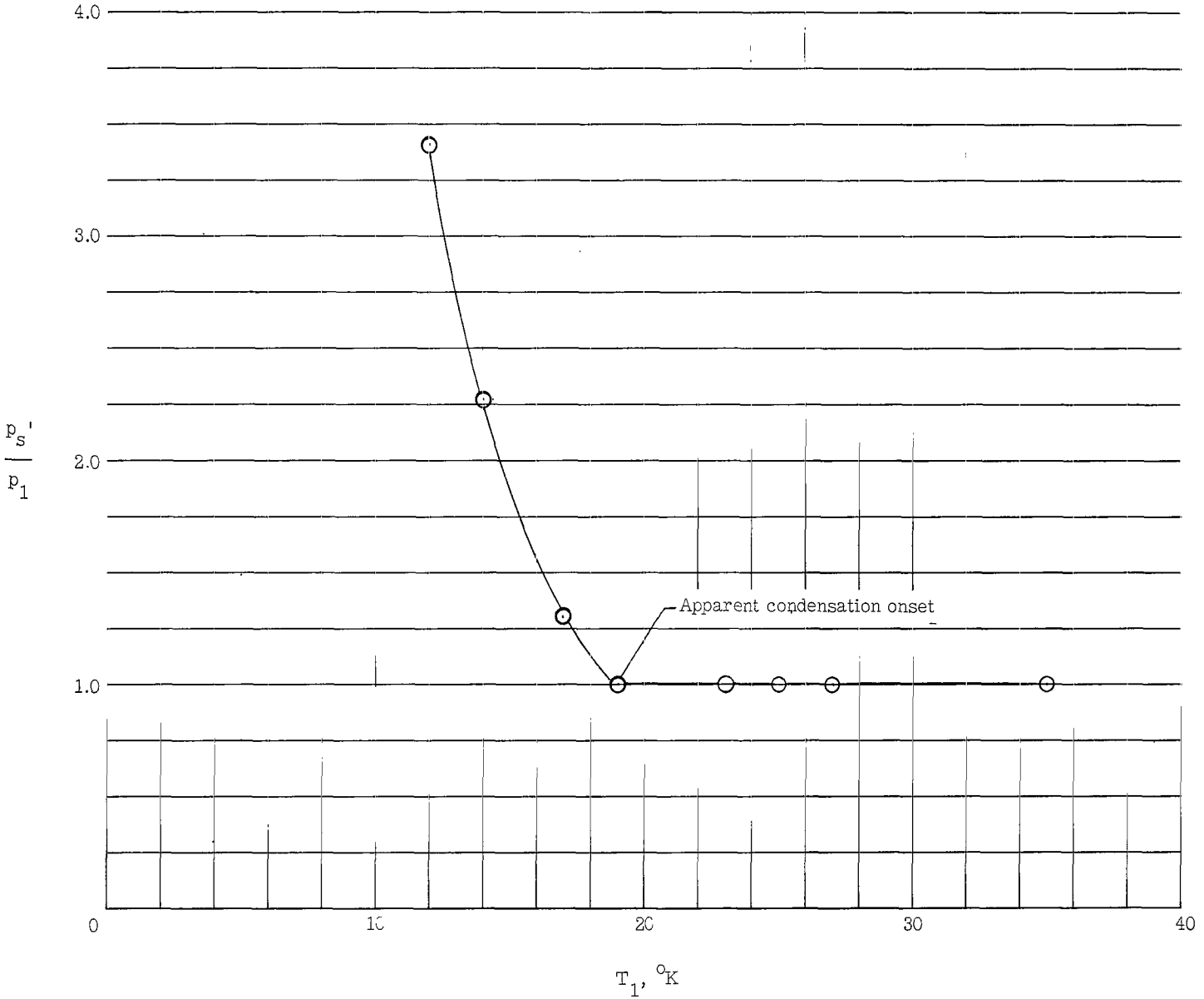

Figure 21.- Effect of condensation on flat-plate surface pressure for $p \approx 0.001$ psi $(6.89\ N/m^2)$.

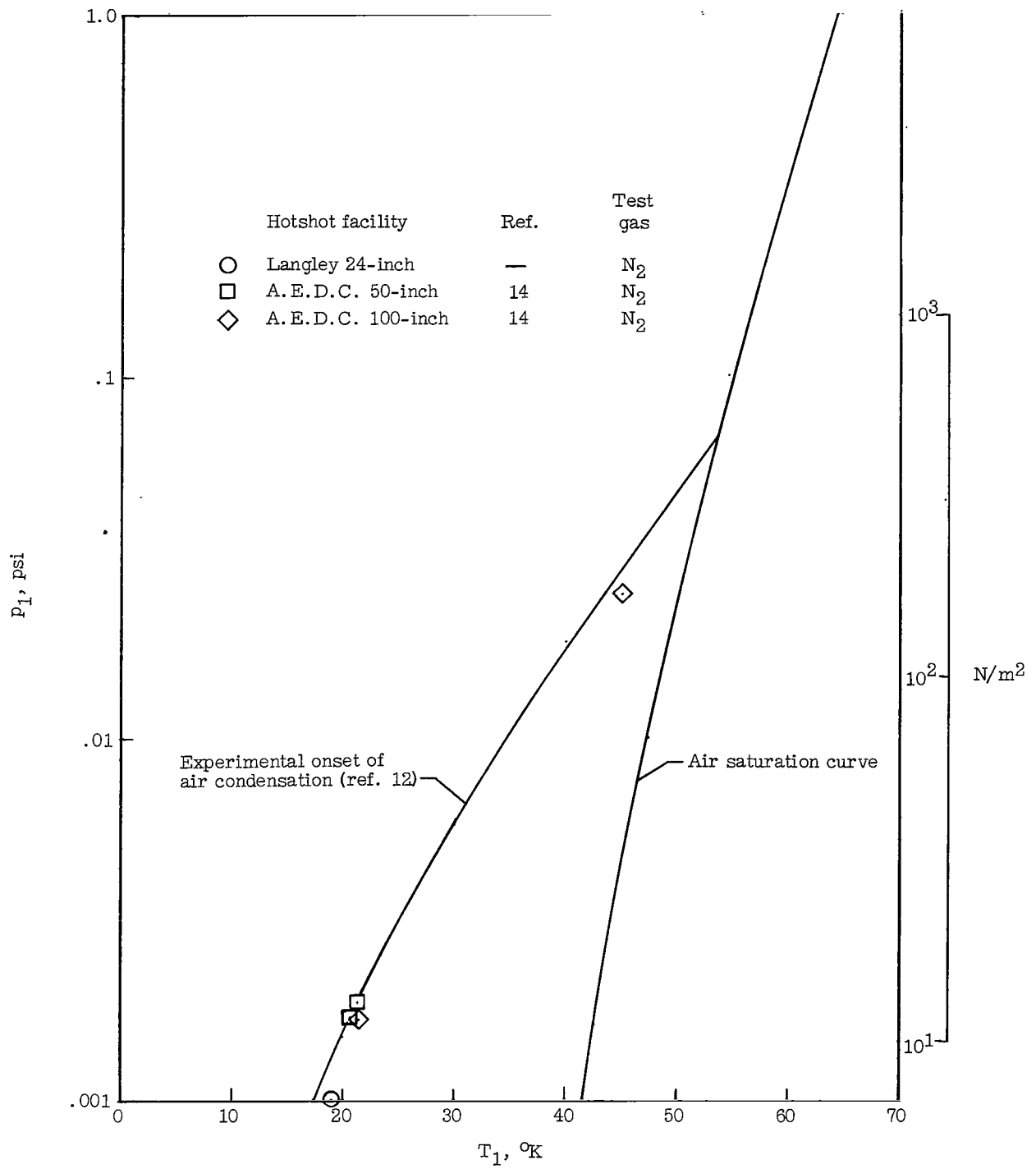

Figure 22.- Free-stream static-pressure and temperature conditions at condensation onset.

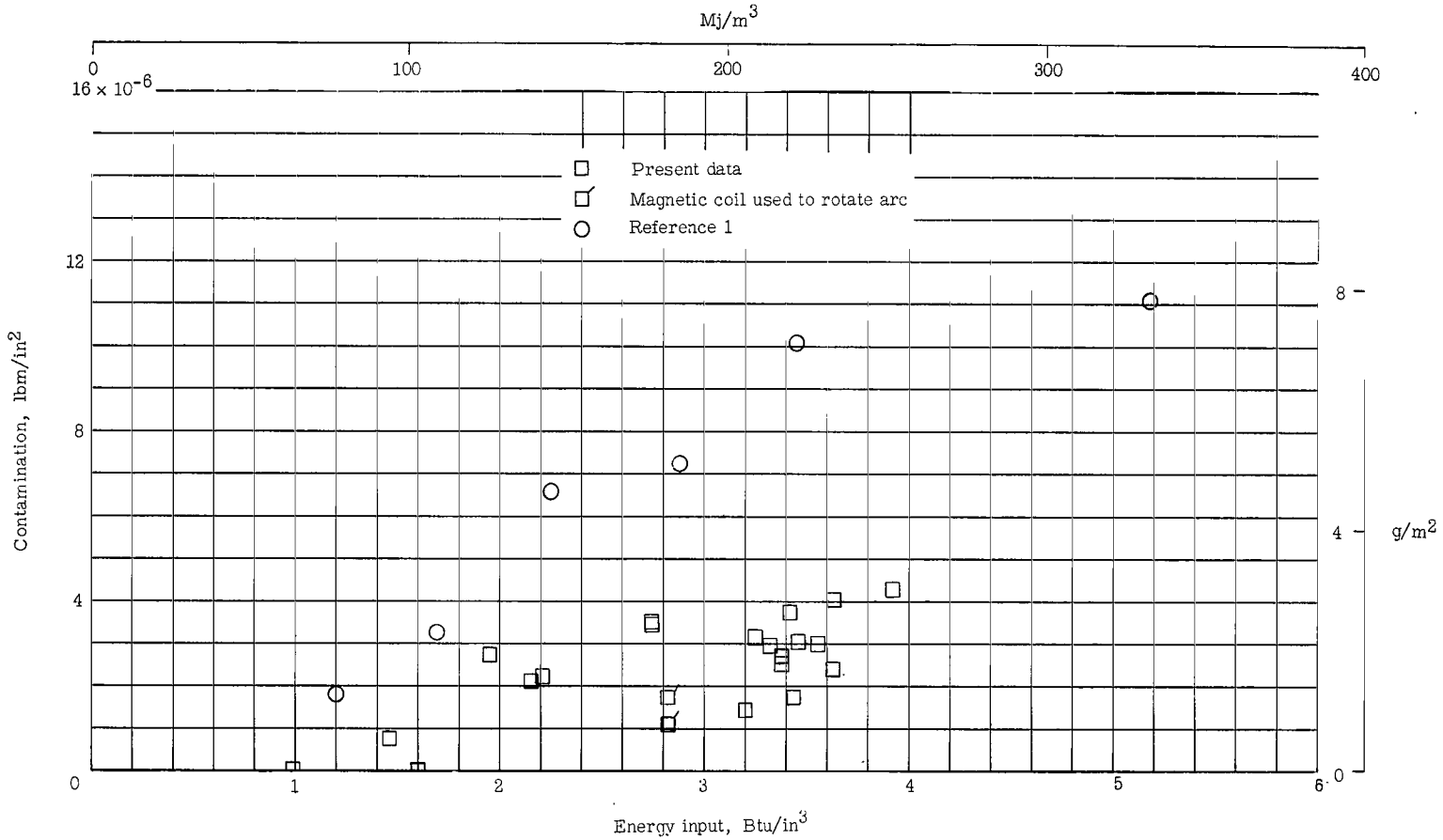

Figure 23.- Solid-contamination results in the Langley hotshot tunnel.

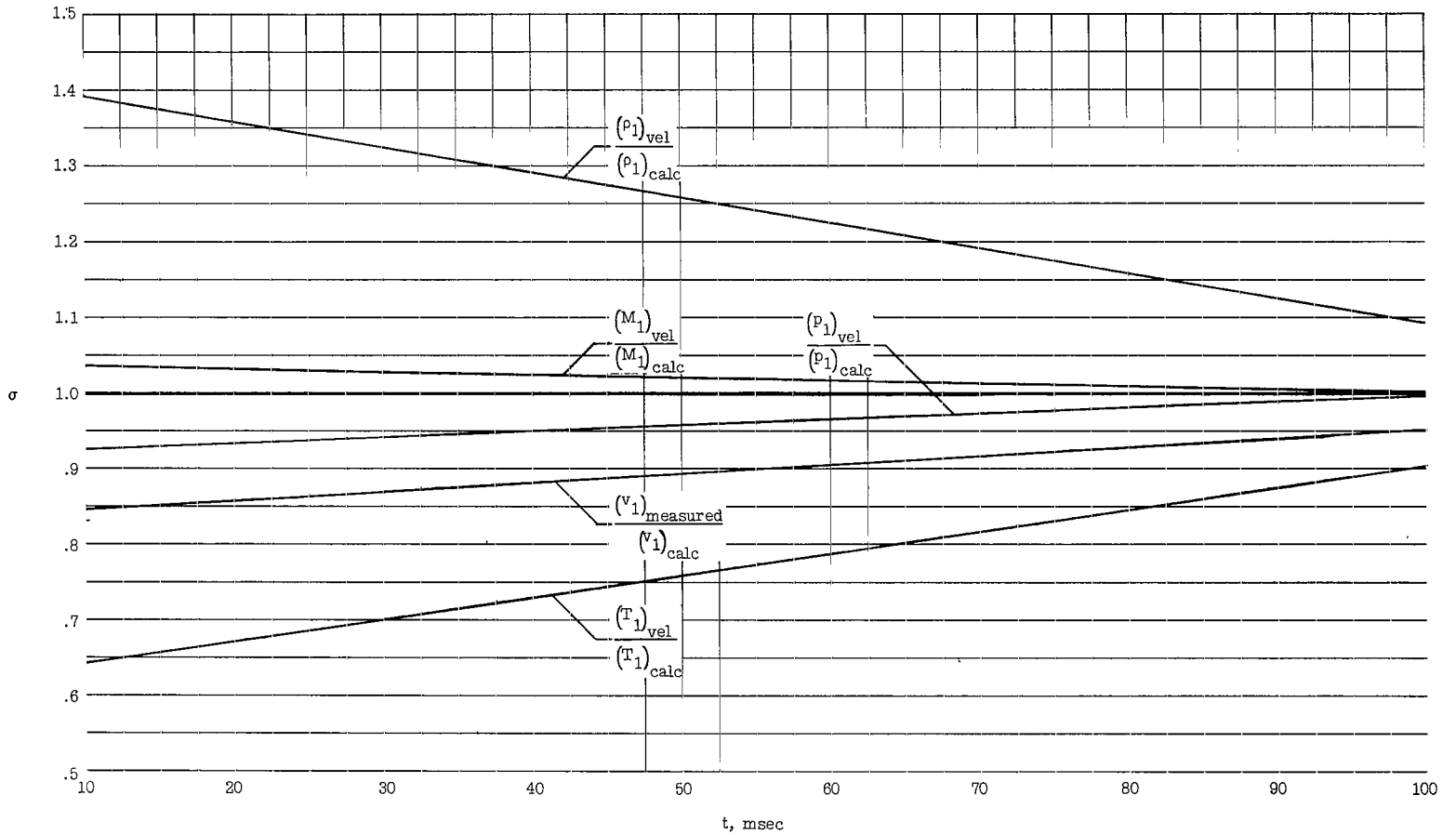

Figure 24.- Variation of ratio of measured velocity-corrected parameters to uncorrected parameters with time. d* = 0.100 (2.54 mm).

"The aeronautical and space activities of the United States shall be conducted so as to contribute . . . to the expansion of human knowledge of phenomena in the atmosphere and space. The Administration shall provide for the widest practicable and appropriate dissemination of information concerning its activities and the results thereof."

—NATIONAL AERONAUTICS AND SPACE ACT OF 1958

NASA SCIENTIFIC AND TECHNICAL PUBLICATIONS

TECHNICAL REPORTS: Scientific and technical information considered important, complete, and a lasting contribution to existing knowledge.

TECHNICAL NOTES: Information less broad in scope but nevertheless of importance as a contribution to existing knowledge.

TECHNICAL MEMORANDUMS: Information receiving limited distribution because of preliminary data, security classification, or other reasons.

CONTRACTOR REPORTS: Technical information generated in connection with a NASA contract or grant and released under NASA auspices.

TECHNICAL TRANSLATIONS: Information published in a foreign language considered to merit NASA distribution in English.

TECHNICAL REPRINTS: Information derived from NASA activities and initially published in the form of journal articles.

SPECIAL PUBLICATIONS: Information derived from or of value to NASA activities but not necessarily reporting the results of individual NASA-programmed scientific efforts. Publications include conference proceedings, monographs, data compilations, handbooks, sourcebooks, and special bibliographies.

Details on the availability of these publications may be obtained from:

SCIENTIFIC AND TECHNICAL INFORMATION DIVISION

NATIONAL AERONAUTICS AND SPACE ADMINISTRATION

Washington, D.C. 20546